Time-Coordinated Path Following of Multiple UAVs over Time-Varying Networks using $\mathcal{L}_1$ Adaptation*

A. P. Aguiar † and A. M. Pascoal ‡
Instituto Superior Técnico, Lisbon, Portugal

I. Kaminer § and V. Dobrokhodov ¶
Naval Postgraduate School, Monterey, CA 93943

E. Xargay ‖ and N. Hovakimyan **
University of Illinois at Urbana-Champaign, Urbana, IL 61801

C. Cao ††
University of Connecticut, Storrs, CT 06269

R. Ghabcheloo ‡‡
Tampere University of Technology, Tampere, Finland

Motivated by challenging mission scenarios, this paper tackles the problem of multi-Unmanned Aerial Vehicle (UAV) cooperative control in the presence of time-varying communication networks. Specifically, we address the problem of steering a fleet of UAVs along given paths (path following) so as to meet spatial and/or temporal constraints. One possible scenario is the situation where a fleet of vehicles is tasked to execute collision-free maneuvers under strict spatial constraints and arrive at their final destinations at exactly the same time. The paper builds on previous work by the authors on coordinated path following and extends it to allow for time-varying communication topologies.

Path following control in 3D builds on a nonlinear control strategy that is first derived at the kinematic level (outer-loop control). This is followed by the design of an $\mathcal{L}_1$ adaptive output feedback control law that effectively augments an existing autopilot and yields an inner-outer loop control structure with guaranteed performance. Multiple vehicle time-critical coordination is achieved by enforcing temporal constraints on the speed profiles of the vehicles along their paths in response to information exchanged over a dynamic communication network. We address explicitly the situation where each vehicle transmits its coordination state to only a subset of the other vehicles, as determined by the communications topology adopted. Further, we consider the case where the communication graph that captures the underlying communication network topology may be disconnected during some interval of time (or may even fail to be connected at any instant of time) and provide conditions under which the complete coordinated path following closed-loop system is stable. Hardware-in-the-Loop (HITL) simulations results demonstrate the benefits of the algorithms developed.

*Research supported in part by projects GREX / CEC-IST (Contract No. 035223), NAV-Control / FCT-PT (PTDC/EEA-ACR/65996/2006), FREESUBNET RTN of the CEC, the FCT-ISR/IST plurianual funding program through the POS_C Program that includes FEDER funds, USSOCOM, ONR under Contract N00014-05-1-0828, AFOSR under Contract No. FA9550-05-1-0157, and ARO under Contract No. W911NF-06-1-0330.

†Assistant Professor, Institute for Systems and Robotics & Electrical Engineering and Computers, Instituto Superior Técnico, Portugal, AIAA Member; pedro@isr.ist.utl.pt.

‡Associate Professor, Institute for Systems and Robotics & Electrical Engineering and Computers, Instituto Superior Técnico, Portugal, AIAA Member; antonio@isr.ist.utl.pt.

§Professor, Department of Mechanical & Astronautical Engineering, Naval Postgraduate School, AIAA Member; kaminer@nps.edu.

¶Research Assistant Professor, Department of Mechanical & Astronautical Engineering, Naval Postgraduate School, AIAA Member; vldobr@nps.edu.

‖Graduate Student, Department of Mechanical Science & Engineering, University of Illinois at Urbana-Champaign, AIAA Student Member; xargay@illinois.edu.

**Professor, Department of Mechanical Science & Engineering, University of Illinois at Urbana-Champaign, AIAA Associate Fellow; nhovakim@illinois.edu.

††Research Assistant Professor, Department of Mechanical Engineering, University of Connecticut, AIAA Member; ccao@engr.uconn.edu

‡‡Senior Researcher, Department of Intelligent Hydraulics and Automation, Tampere University of Technology, Finland; reza.ghabcheloo@tut.fi

I. Introduction

Unmanned Aerial Vehicles (UAVs) are becoming ubiquitous and play an increasingly important role in military reconnaissance and strike operations, border patrol missions, forest fire detection, police surveillance, and recovery operations, to name but a few. In simple applications, a single autonomous vehicle can be managed by a crew using a ground station provided by the vehicle manufacturer. The execution of more challenging missions, however, requires the use of multiple vehicles working in cooperation to achieve a common objective. Representative examples of cooperative mission scenarios are sequential auto-landing and coordinated ground target suppression for multiple UAVs. The first refers to the situation where a fleet of UAVs must break up and arrive at the assigned glideslope point, separated by pre-specified safe-guarding time-intervals. In the case of ground target suppression, a formation of UAVs must again break up and execute a coordinated maneuver to arrive at a predefined position over the target at the same time.

In both cases, no absolute temporal constraints are given *a priori* - a critical point that needs to be emphasized. Furthermore, the vehicles must execute maneuvers in close proximity to each other. In addition, as pointed out in Refs.[1,2], the flow of information among vehicles may be severely restricted, either for security reasons or because of tight bandwidth limitations. As a consequence, no vehicle will be able to communicate with the entire formation and the inter-vehicle communication network may change over time. Under these circumstances, it is important to develop coordinated motion control strategies that can yield robust performance in the presence of time varying communication networks arising from communication failures and switching communication topologies.

Motivated by these and similar problems, over the past few years there has been increasing interest in the study of multi-agent system networks with application to engineering and science problems. The range of topics addressed include parallel computing[3], synchronization of oscillators[4], study of collective behavior and flocking[5], multi-system consensus mechanisms[6], multi-vehicle system formations[7], coordinated motion control[8], asynchronous protocols[9], dynamic graphs[10], stochastic graphs[10–12], and graph-related theory[2,13]. Especially relevant are the applications of the theory developed in the area of multi-vehicle formation control: spacecraft formation flying[14], unmanned aerial vehicle (UAV) control[15,16], coordinated control of land robots[8], and control of multiple autonomous underwater vehicles (AUVs)[17,18]. In spite of significant progress in these challenging areas, much work remains to be done to develop strategies capable of yielding robust performance of a fleet of vehicles in the presence of complex vehicle dynamics, communication constraints, and partial vehicle failures.

In Ref.[19], a general framework for the problem of coordinated control of multiple autonomous vehicles that must operate under strict spatial and temporal constraints was presented. The framework proposed borrows from multiple disciplines and integrates algorithms for path generation, path following, time-critical coordination, and $\mathcal{L}_1$ adaptive control theory for fast and robust adaptation. Together, these techniques yield control laws that meet strict performance requirements in the presence of modeling uncertainties and environmental disturbances. The methodology proposed in Ref.[19] is exemplified for the case of UAVs and unfolds in three basic steps. First, given a multiple vehicle task, a set of feasible trajectories are generated for all UAVs using an expedite method that takes explicitly into account the initial and final boundary conditions, a general performance criterion to be optimized, the simplified UAV dynamics, and safety rules for collision avoidance. The second step consists of making each vehicle follow its assigned path while tracking a desired speed profile. Path following control design is first done at a kinematic level, leading to an outer-loop controller that generates pitch and yaw rate commands to an inner-loop controller. The latter relies on off-the-shelf autopilots for angular rate command tracking, augmented with an $\mathcal{L}_1$ adaptive output feedback control law that guarantees stability and performance of the complete system for each vehicle in the presence of modeling uncertainties and environmental disturbances. Finally, in the third step the speed profile of each vehicle is adjusted about the nominal speed profile derived in the first step to enforce the temporal constraints that must be met in real-time in order to coordinate the entire fleet of UAVs. In this step, it is assumed that the vehicles exchange information over a fixed communication network.

The present paper builds on the work reported in Ref.[19] but departs considerably from it in that it allows for the consideration of time-varying communication networks. In particular, we address explicitly the case where the communication graph that captures the underlying communication network topology may be disconnected during some interval of time or may even fail to be connected at any instant of time. We show rigorously that if the desired speed profiles of the vehicles along their paths are constant and the connectivity of the communication graph satisfies a certain persistency of excitation (PE) condition, then the UAVs reach agreement. HITL simulation results demonstrate the benefits of the algorithms developed.

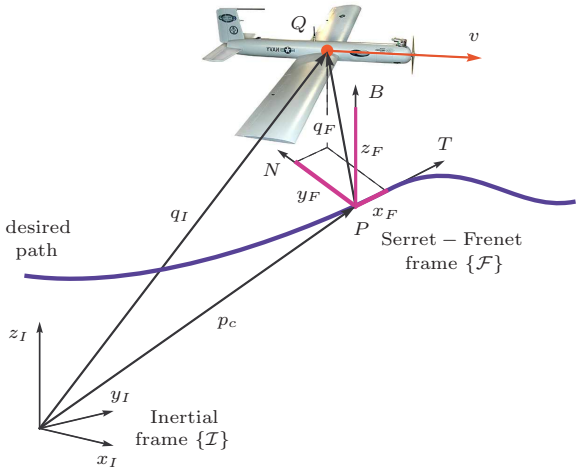

Figure 1. Problem geometry

The paper is organized as follows. Section II presents a path following algorithm for UAVs in 3D space. At this stage, path following is done at the kinematic level (outer-loop control). Section III derives a strategy for time-coordinated control of multiple UAVs in the presence of time-varying communication topologies that relies on the adjustment of the desired speed profile of each vehicle. Section IV describes an $\mathcal{L}_1$ adaptive augmentation technique both for path following and time coordination that yields an inner-loop control structure and exploits the availability of off-the-shelf autopilots. Sections V and VI solve the problem of coordinated path following taking into account the UAV dynamics. Section VII describes HILT simulation results and includes a briefly description of the hardware used in the configuration. The paper ends with the conclusions in Section VIII.

II. Path Following in 3D Space

This section describes an algorithm for UAV path following in 3D space. We recall that a path is simply a curve $p_c : \tau \to \mathbb{R}^3$ parameterized by τ in a closed subset of $\mathbb{R}_+$, that is, $p_c = p_c(\tau)$. If τ is identified with time t or is a function thereof, then, and with a slight abuse of notation, $p_c(t) = p_c(\tau(t))$ will be called a trajectory. Path following refers to the problem of making a vehicle converge to and follow a path $p_c(\tau)$ with no assigned time schedule. However, the vehicle speed may be assigned as a function of the parameter τ.

In what follows we avail ourselves of the results derived in Ref.[20] (see also Refs.[21,22]) where an algorithm was proposed to generate space deconflicting feasible paths for multiple AUVs, that is, paths $p_{c_i}(\tau)$ that do not intersect each other and that yield trajectories that can be tracked by an UAV without exceeding prespecified bounds on its velocity and total acceleration along that trajectory.

In order for the ith vehicle to follow the spatial path $p_{c_i}(\tau)$ using the algorithm in Ref.[20] , a path following algorithm that extends the one in Ref.[23] to a 3D setting with a further modification aimed at meeting time-critical and inter-vehicle constraints is now presented. At this level, only the simplified kinematic equations of the vehicle will be addressed by taking pitch rate and yaw rate as virtual outer-loop control inputs. The dynamics of the closed-loop UAV with autopilot are dealt with in Sections V and VI by introducing an inner-loop control law via the novel $\mathcal{L}_1$ adaptive output feedback controller.

Figure 1 captures the geometry of the problem at hand. Let $\mathcal{I}$ denote an inertial frame. Let Q be the UAV center of mass. Further, let $p_c(l)$ be the path to be followed, parameterized by its path length l, and P be an arbitrary point on the path that plays the role of the center of mass of a virtual UAV to be followed. Note that this is a different approach as compared to the set-up for path following originally proposed in Ref.[24] , where P was simply defined as the point on the path that is closest to the vehicle. Endowing P with an extra degree of freedom is the key to the algorithm presented in Ref.[23] .

Let $\mathcal{F}$ be a Serret-Frenet frame attached to the point P on the path, and let $T(l)$, $N(l)$ and $B(l)$, defined

as

$$\begin{aligned} T(l) &= \frac{dp_c(l)}{dl} \Big/ \left\| \frac{dp_c(l)}{dl} \right\|, \\ N(l) &= \frac{dT(l)}{dl} \Big/ \left\| \frac{dT(l)}{dl} \right\|, \\ B(l) &= T(l) \times N(l), \end{aligned}$$

be an orthonormal basis for $\mathcal{F}$. We recall that these unit vectors define the tangent, normal, and binormal directions, respectively to the path at the point determined by l. They can be used to construct the rotation matrix $R_F^I = [T\ N\ B]$ from $\mathcal{F}$ to $\mathcal{I}$. Denote by ω_{FI}^F the angular velocity of $\mathcal{F}$ with respect to $\mathcal{I}$, resolved in $\mathcal{F}$, given by

$$\omega_{FI}^F = \left[\zeta(l)\dot{l}\ 0\ \kappa(l)\dot{l}\right]^\top,$$

where $\kappa(l) = \left\| \frac{dT(l)}{dl} \right\|$ is the curvature of the path and $\zeta(l) = \left\| \frac{dB(l)}{dl} \right\|$ is its torsion. Let

$$q_I(t) = [x_I(t)\ y_I(t)\ z_I(t)]^\top$$

be the position of the UAV center of mass Q resolved in $\mathcal{I}$, and let

$$q_F(t) = [x_F(t)\ y_F(t)\ z_F(t)]^\top$$

be the difference between $q_I(t)$ and $p_c(t)$ resolved in $\mathcal{F}$. Finally, let $\mathcal{W}'$ denote a coordinate system defined by projecting the wind frame $\mathcal{W}$ onto a local level plane. (The frame $\mathcal{W}$ has its origin at Q and its x-axis is aligned with the UAV's velocity vector).

Let

$$\Phi_e(t) = [\phi_e(t)\ \theta_e(t)\ \psi_e(t)]^\top$$

denote the Euler angles that locally parameterize the rotation matrix from $\mathcal{F}$ to $\mathcal{W}'$. In what follows, $v(t)$ is the magnitude of the UAV's velocity vector, $\gamma(t)$ is the flight path angle, $\psi(t)$ is the ground heading angle, and $q(t)$ and $r(t)$ are the x-axis and z-axis components, respectively, of the vehicle's rotational velocity resolved in $\mathcal{W}'$ frame. For the purpose of this paper and with a slight abuse of notation, $q(t)$ and $r(t)$ will be referred to as *pitch rate* and *yaw rate*, respectively, in the $\mathcal{W}'$ frame.

With the above notation, the UAV kinematic equations can be written as

$$\begin{cases} \dot{x}_I = v\cos\gamma\cos\psi \\ \dot{y}_I = -v\cos\gamma\sin\psi \\ \dot{z}_I = v\sin\gamma \\ \begin{bmatrix} \dot{\gamma} \\ \dot{\psi} \end{bmatrix} = \begin{bmatrix} 1 & 0 \\ 0 & \cos^{-1}\gamma \end{bmatrix} \begin{bmatrix} q \\ r \end{bmatrix} \end{cases}.$$

Straightforward computations[a] yield the dynamic equations of the path following kinematic error states as

$$\mathcal{G}_e : \begin{cases} \dot{x}_F = -\dot{l}(1-\kappa(l)y_F) + v\cos\theta_e\cos\psi_e \\ \dot{y}_F = -\dot{l}(\kappa(l)x_F - \zeta(l)z_F) + v\cos\theta_e\sin\psi_e \\ \dot{z}_F = -\dot{l}\zeta(l)y_F - v\sin\theta_e \\ \begin{bmatrix} \dot{\theta}_e \\ \dot{\psi}_e \end{bmatrix} = D(t,\theta_e,\psi_e) + T(t,\theta_e) \begin{bmatrix} q \\ r \end{bmatrix} \end{cases} \quad (1)$$

[a] See Ref.[20] for details in the derivation of these dynamics.

where

$$D\left(t,\theta_e,\psi_e\right) = \begin{bmatrix} \dot{l}\zeta(l)\sin\psi_e \\ -\dot{l}(\zeta(l)\tan\theta_e\cos\psi_e+\kappa(l)) \end{bmatrix} \tag{2}$$

$$T\left(t,\theta_e\right) = \begin{bmatrix} \cos\phi_e & -\sin\phi_e \\ \frac{\sin\phi_e}{\cos\theta_e} & \frac{\cos\phi_e}{\cos\theta_e} \end{bmatrix}. \tag{3}$$

Note that, in the kinematic error model (1), $q(t)$ and $r(t)$ play the role of "virtual" control inputs. Notice also how the rate of progression $\dot{l}(t)$ of the point P along the path becomes an extra variable that can be manipulated at will.

At this point, it is convenient to formally define the state vector for the path following kinematic dynamics as

$$x(t) = \begin{bmatrix} x_F(t) & y_F(t) & z_F(t) & \theta_e(t)-\delta_\theta(t) & \psi_e(t)-\delta_\psi(t) \end{bmatrix}^\top,$$

where

$$\begin{aligned} \delta_\theta(t) &= \sin^{-1}\left(\frac{z_F(t)}{|z_F(t)|+d_1}\right), \\ \delta_\psi(t) &= \sin^{-1}\left(\frac{-y_F(t)}{|y_F(t)|+d_2}\right), \end{aligned} \tag{4}$$

with d_1 and d_2 some positive constants. Notice that, instead of the angular errors $\theta_e(t)$ and $\psi_e(t)$, we use $\theta_e(t)-\delta_\theta(t)$ and $\psi_e(t)-\delta_\psi(t)$ respectively to shape the "approach" angles to the path. Clearly, when the vehicle is far from the desired path the approach angles become close to $\pi/2$. As the vehicle comes closer to the path, the approach angles tend to 0. The system $\mathcal{G}_e$ is completely characterized by defining the vector of input signals as

$$y(t) = \begin{bmatrix} q(t) & r(t) \end{bmatrix}^\top.$$

Next, we show that there exist stabilizing functions for $q(t)$ and $r(t)$ leading to local exponential stability of the origin of $\mathcal{G}_e$ with a prescribed domain of attraction. We start by assuming that the UAV speed satisfies the lower bound

$$v_{\min} \leq v(t), \quad \forall\, t \geq 0. \tag{5}$$

Let c_1 and c_2 be arbitrary positive constants satisfying the following condition

$$\nu_i \triangleq \sqrt{cc_2}+\sin^{-1}\left(\frac{\sqrt{cc_1}}{\sqrt{cc_1}+d_i}\right) \leq \frac{\pi}{2}-\epsilon_i, \quad i=1,2 \tag{6}$$

where $c>0$ is any positive constant, d_1 and d_2 were introduced in (4), and ϵ_1 and ϵ_2 are positive constants such that $0<\epsilon_i<\frac{\pi}{2}$, $i=1,2$. Let the rate of progression of the point P along the path be governed by

$$\dot{l}(t) = K_1 x_F(t)+v(t)\cos\theta_e(t)\cos\psi_e(t), \tag{7}$$

where $K_1>0$. Then, the input vector $y_c(t)$ given by

$$y_c(t) = \begin{bmatrix} q_c(t) \\ r_c(t) \end{bmatrix} = T^{-1}\left(t,\theta_e\right)\left(\begin{bmatrix} u_{\theta_c}(t) \\ u_{\psi_c}(t) \end{bmatrix} - D\left(t,\theta_e,\psi_e\right)\right), \tag{8}$$

where $D\left(t,\theta_e,\psi_e\right)$ and $T\left(t,\theta_e\right)$ were introduced in (2) and (3), and $u_{\theta_c}(t)$ and $u_{\psi_c}(t)$ are defined as

$$\begin{aligned} u_{\theta_c}(t) &= -K_2\left(\theta_e(t)-\delta_\theta(t)\right)+\frac{c_2}{c_1}z_F(t)v(t)\frac{\sin\theta_e(t)-\sin\delta_\theta(t)}{\theta_e(t)-\delta_\theta(t)}+\dot{\delta}_\theta(t) \\ u_{\psi_c}(t) &= -K_3\left(\psi_e(t)-\delta_\psi(t)\right)-\frac{c_2}{c_1}y_F(t)v(t)\cos\theta_e(t)\frac{\sin\psi_e(t)-\sin\delta_\psi(t)}{\psi_e(t)-\delta_\psi(t)}+\dot{\delta}_\psi(t), \end{aligned} \tag{9}$$

stabilize the subsystem $\mathcal{G}_e$ for any $K_2>0$ and $K_3>0$. Figure 2 presents the kinematic closed-loop system. A formal statement of this key result is given in the lemma below.

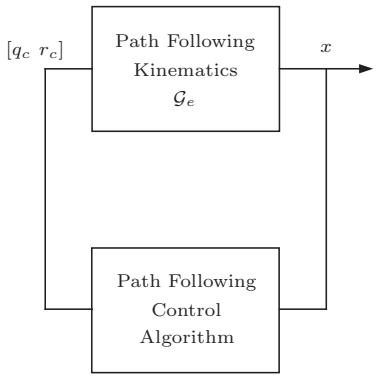

Figure 2. Path following closed-loop system for a single UAV solved at a kinematic level

Lemma 1 *Let $d = \sqrt{cc_1}$, where c and c_1 were introduced in (6). Further, let the progression of the point P along the path be governed by (7). Then, for any $v(t)$ verifying (5), the origin of the kinematic error equations in (1) with the controllers $q(t) \equiv q_c(t)$, $r(t) \equiv r_c(t)$ defined in (8)-(9) is exponentially stable with the domain of attraction*

$$\Omega \;=\; \left\{ x \;:\; V_p(x) < \frac{c}{2} \right\}, \tag{10}$$

where

$$\begin{aligned} V_p(x) &= x^\top P_p x \\ P_p &= \operatorname{diag}\left(\frac{1}{2c_1}, \frac{1}{2c_1}, \frac{1}{2c_1}, \frac{1}{2c_2}, \frac{1}{2c_2} \right). \end{aligned}$$

Proof. If $q(t) \equiv q_c(t)$ and $r(t) \equiv r_c(t)$, it is easy to check from (1) and (8) that

$$\begin{aligned} \dot{\theta}_e(t) &= u_{\theta_c}(t), \\ \dot{\psi}_e(t) &= u_{\psi_c}(t). \end{aligned}$$

Then, it follows from (1), (4), (7), and (8)-(9) that

$$\dot{V}_p \;=\; -x^\top Q_p x\,,$$

with

$$Q_p = \operatorname{diag}\left(\frac{K_1}{c_1} \;\; \frac{v\cos\theta_e}{c_1(|y_F| + d_2)} \;\; \frac{v}{c_1(|z_F| + d_1)} \;\; \frac{K_2}{c_2} \;\; \frac{K_3}{c_2} \right). \tag{11}$$

Note that over the compact set Ω the following upper bounds hold

$$\begin{aligned} |x_F(t)| &< d, \\ |y_F(t)| &< d, \\ |z_F(t)| &< d, \\ |\theta_e(t)| &< \sqrt{cc_2} + |\delta_\theta(t)| < \sqrt{cc_2} + \sin^{-1}\left(\frac{d}{d+d_1} \right) = \nu_1 < \frac{\pi}{2}, \\ |\psi_e(t)| &< \sqrt{cc_2} + |\delta_\psi(t)| < \sqrt{cc_2} + \sin^{-1}\left(\frac{d}{d+d_2} \right) = \nu_2 < \frac{\pi}{2}, \end{aligned} \tag{12}$$

where we have used the relationship (6). Now it follows from (11) and (12) that $Q_p \geq \bar{Q}_p$, where

$$\bar{Q}_p = \operatorname{diag}\left(\frac{K_1}{c_1} \;\; \frac{v_{\min}\cos\nu_1}{c_1(d+d_2)} \;\; \frac{v_{\min}}{c_1(d+d_1)} \;\; \frac{K_2}{c_2} \;\; \frac{K_3}{c_2} \right). \tag{13}$$

Since $\bar{Q}_p > 0$ and

$$\dot{V}_p(x) \quad \leq \quad -x^\top \bar{Q}_p x\,, \qquad \forall\, t \geq 0\,,$$

$x(t)$ converges exponentially to zero over the compact set Ω. Then, it follows from the definitions in (4) that both $\delta_\theta(t)$ and $\delta_\psi(t)$ converge exponentially to zero, and thus one finds that $\theta_e(t)$ and $\psi_e(t)$ also converge exponentially to zero, which completes the proof.

A more detailed derivation of this proof can be found in Ref.[25] . □

Remark 1 *The control law (8)-(9) produces angular rate commands defined in $\mathcal{W}'$ frame. However, a typical commercial autopilot accepts rate commands defined in body-fixed frame $\mathcal{B}$. The coordinate transformation from $\mathcal{W}'$ to $\mathcal{B}$ is given by*

$$R^B_{W'} \quad = \quad R^B_W R^W_{W'}\,,$$

where the transformation R^B_W is defined using the angle of attack and the sideslip angle. For the UAVs considered in this paper, these angles are usually small, and therefore it is reasonable to assume that $R^B_W \approx \mathbb{I}$. On the other hand, $R^W_{W'}$ is defined via a single rotation around a local x-axis by an angle ϕ_W. For small values of angle of attack and sideslip angle, ϕ_W can be approximated by the body-fixed bank angle ϕ measured by a typical autopilot. Therefore, in the final implementation, the angular rate commands (8)-(9) are resolved in the body-fixed frame $\mathcal{B}$ using the transformation discussed here.

Thus, in the following sections we assume that both the autopilot angular rates $y(t) = [q(t)\ r(t)]^\top$ and the commanded angular rates $y_c(t) = [q_c(t)\ r_c(t)]^\top$ are resolved in $\mathcal{W}'$. We notice that this assumption will not affect the results since, for small angle of attack and the sideslip angle, we have

$$\|(y(t) - y_c(t))^{W'}\|_2 \quad \approx \quad \|(y(t) - y_c(t))^{B}\|_2\,.$$

III. Time-Critical Coordination

Having solved the path following problem for a single vehicle and an arbitrary speed profile at a kinematic level, we now address the problem of time-coordinated control of multiple vehicles. Examples of applications in which this would be useful include situations where all vehicles must arrive at their final destinations at exactly the same time, or at different times so as to meet a desired inter-vehicle arrival schedule. Without loss of generality, we consider the problem of simultaneous arrival. Let t_f be the arrival time of the first UAV. Denote l_{f_i} as the total length of the spatial path for the ith UAV. In addition, let $l_i(t)$ be the path length from the origin to $p_i(t)$ along the spatial path of the ith UAV. Define $l'_i(t) = l_i(t)/l_{fi}$. Clearly, $l'_i(t_f) = 1$ for $i = 1, 2, \ldots, n$ implies that all vehicles arrive at their final destination at the same time. Since $\dot{l}'_i(t) = \dot{l}_i(t)/l_{fi}$, it follows from (7) that

$$\dot{l}'_i(t) \quad = \quad \frac{K_1 x_{F_i}(t) + v_i(t)\cos\theta_{e,i}(t)\cos\psi_{e,i}(t)}{l_{fi}}\,, \tag{14}$$

where for simplicity we have kept K_1 without indexing.

To account for the communication constraints, we introduce the neighborhood set J_i that denotes the set of vehicles that the ith vehicle exchanges information with. We impose the constraint that each UAV only exchanges its coordination parameter $l'_i(t)$ with its neighbors according to the topology of the communications.

Then, to solve the coordination problem, we propose the following desired speed profile for the ith UAV[20]

$$v_{c_i}(t) \quad = \quad \frac{u_{\text{coord}_i}(t) l_{fi} - K_1 x_{F_i}(t)}{\cos\theta_{e,i}(t)\cos\psi_{e,i}(t)}\,, \qquad i = 1, \ldots, n\,, \tag{15}$$

with the following decentralized coordination law

$$\begin{aligned}
u_{\text{coord}_1}(t) &= -a\sum_{j\in J_1}(l'_1(t) - l'_j(t)) + \tfrac{v_{d_1}}{l_{f_1}} \\
u_{\text{coord}_i}(t) &= -a\sum_{j\in J_i}(l'_i(t) - l'_j(t)) + \chi_{I_i}(t)\,, && i = 2, \ldots, n \\
\dot{\chi}_{I,i}(t) &= -b\sum_{j\in J_i}(l'_i(t) - l'_j(t))\,, \quad \chi_{I_i}(0) = \tfrac{v_{d_i}}{l_{f_i}} && i = 2, \ldots, n
\end{aligned}$$

where we have elected vehicle 1 as the formation leader, v_{d_1} denotes its desired constant speed profile, v_{d_i}, $i = 2, \ldots, n$, is the speed profile of the follower vehicles, and a, b are positive constants. Note that the coordination control law has a Proportional-Integral (PI) structure, thus allowing each vehicle to learn the speed of the leader, rather than having it available *a priori*.

The coordination law can be re-written in compact form as

$$u_{\text{coord}}(t) = -aL(t)l'(t) + \begin{bmatrix} v_{d_1}/l_{f_1} \\ \chi_I(t) \end{bmatrix}, \tag{16}$$

$$\dot{\chi}_I(t) = -bC^\top L(t)l'(t), \quad \chi_{I_i}(0) = \frac{v_{d_i}}{l_{f_i}} \tag{17}$$

where $l'(t) = [l'_1(t) \ \ldots \ l'_n(t)]^\top$, $u_{\text{coord}}(t) = [u_{\text{coord}_1}(t) \ \ldots \ u_{\text{coord}_n}(t)]^\top$, $\chi_I(t) = [\chi_{I_2}(t) \ \ldots \ \chi_{I_n}(t)]^\top$, $C^\top = [\ 0 \quad I_{n-1}\ ]$, and the $n \times n$ piecewise-continuous matrix $L(t)$ can be interpreted as the Laplacian of an undirected graph $\Gamma(t)$ that captures the underlying bidirectional communication network topology of the UAV formation at time t. It is well known that $L^\top = L$, $L \geq 0$, $L1_n = 0$, and that the second smallest eigenvalue of L is strictly positive, that is,

$$\min_{\substack{x \neq 0 \\ 1_n^\top x = 0}} \frac{x^\top L x}{\|x\|^2} = \lambda_2(L) > 0$$

if and only if the graph Γ is connected (see e.g., Ref.[26]).

In preparation for the development that follows, next we reformulate the coordination problem stated above into a stabilization problem. To this aim, we introduce the following notation: let

$$\Pi \triangleq \mathbb{I}_n - \frac{1_n 1_n^\top}{n}$$

denote the *projection matrix* and Q be a $(n-1) \times n$ matrix such that

$$Q1_n = 0, \quad QQ^\top = \mathbb{I}_{n-1}.$$

Notice that $Q^\top Q = \Pi$, $\Pi = \Pi^\top = \Pi^2$, $L\Pi = \Pi L = L$, and the spectrum of the matrix $\bar{L} \triangleq QLQ^\top$ is equal to the spectrum of L without the eigenvalue $\lambda = 0$ correspondent to the eigenvector 1_n. Define the state variables $\zeta(t) = \left[\zeta_1(t)^\top \ \zeta_2(t)^\top\right]^\top$ as

$$\zeta_1(t) = Q\, l'(t)$$

$$\zeta_2(t) = \chi_I(t) - \frac{v_{d_1}(t)}{l_{f_1}} 1_{n-1},$$

where by definition $\zeta_1(t) = 0 \Leftrightarrow l' \in \text{span}\{1_n\}$ which implies that, if $\zeta(t_f) = 0$, then all UAVs arrive at their final destination at the same time.

Thus, setting

$$e_{v_i}(t) = v_i(t) - v_{c_i}(t), \quad i = 1, \ldots, n,$$

where $e_{v_i}(t)$ denotes the velocity error for the ith vehicle in the coordination, it follows from (15) that the kinematic equation (14) can be rewritten as

$$\dot{l}'_i(t) = u_{\text{coord}_i}(t) + \frac{e_{v_i}(t)\cos\theta_{e,i}(t)\cos\psi_{e,i}(t)}{l_{fi}}, \tag{18}$$

and therefore, the closed-loop coordination dynamics formed by (18) and the coordination control algorithm defined in (16)-(17) can be reformulated as

$$\dot{\zeta}(t) = F(t)\zeta(t) + H\varphi(t), \tag{19}$$

where

$$F(t) = \begin{bmatrix} -a\bar{L}(t) & QC \\ -bC^\top Q^\top \bar{L}(t) & 0 \end{bmatrix}$$

$$H = \begin{bmatrix} Q \\ 0 \end{bmatrix},$$

and $\varphi(t) \in \mathbb{R}^n$ is a vector with its ith element $\frac{e_{v_i}(t)\cos\theta_{e,i}(t)\cos\psi_{e,i}(t)}{l_{fi}}$.

Next we show that for fixed or time-varying communication topologies but assuming that the graph remains connected for all $t \geq 0$, if every vehicle travels at the commanded speed $v_{c_i}(t)$ ($e_{v_i}(t) \equiv 0$), then the coordinated system reaches agreement and all the vehicles travel at the same path length rate, that is

$$\begin{aligned} \lim_{t\to\infty} \left(l'_i(t) - l'_j(t)\right) &= 0\,, \qquad \forall i,j \in \{1,\ldots,n\} \\ \lim_{t\to\infty} \dot{l}'(t) &= \frac{v_{d_1}}{l_{f_1}}\,. \end{aligned}$$

On the other hand, if $e_{v_i}(t) \neq 0$, then the error of the disagreement vector degrades gracefully with the size of $|e_{v_i}(t)|$.

Lemma 2 *Consider the coordination system (19) and suppose that the graph that models the communication topology $\Gamma(t)$ is connected for all $t \geq 0$. Then, for any selected rate of convergence $\bar{\lambda} > 0$, there exist a sufficiently large coordinated control gains a, b such that the system (19) is input-to-state stable (ISS) with respect to $e_v(t) = [e_{v_1}(t) \;\cdots\; e_{v_n}]^\top$, that is,*

$$\|\zeta(t)\| \leq k_1 \|\zeta(0)\| e^{-\bar{\lambda}t} + k_2 \sup_{\tau\in[0,t)} \|e_v(\tau)\|\,, \qquad \forall t \geq 0 \tag{20}$$

for some $k_1, k_2 > 0$. Furthermore, the normalized lengths $l'_i(t)$ and path-length rates $\dot{l}'_i(t)$ satisfy

$$\lim_{t\to\infty} \sup \left|l'_i(t) - l'_j(t)\right| \leq k_3 \lim_{t\to\infty} \sup \|e_v(t)\|\,, \tag{21}$$

$$\lim_{t\to\infty} \sup \left|\dot{l}'_i(t) - \frac{v_{d_1}}{l_{f_1}}\right| \leq k_4 \lim_{t\to\infty} \sup \|e_v(t)\|\,, \tag{22}$$

for all $i, j \in \{1,\ldots,n\}$, and for some $k_3, k_4 > 0$.

Proof. To prove ISS we first show that the homogeneous equation of the coordination dynamics

$$\dot{\zeta}(t) = F(t)\zeta(t) \tag{23}$$

is uniformly exponentially stable. To this aim, we consider the Lyapunov function candidate

$$V_c(\zeta(t)) = \zeta(t)^\top P_c \zeta(t) \tag{24}$$

where P_c is defined to have the following structure

$$P_c = \begin{bmatrix} \mathbb{I}_{n-1} & -\frac{\delta}{\lambda n^2} QC \\ -\frac{\delta}{\lambda n^2} C^\top Q^\top & \frac{a\delta}{b\lambda n^2}\mathbb{I}_{n-1} \end{bmatrix}, \tag{25}$$

with $\delta > 0$ being an arbitrary positive constant.

We notice now that, since the graph $\Gamma(t)$ is connected for every $t \geq 0$, it follows that there exists a constant $\delta_c > 0$ such that

$$\lambda_2(L(t)) > \delta_c, \quad \forall t \geq 0\,. \tag{26}$$

If we set $\delta = \delta_c$ in the definition of P_c in (25), then the lower bound in (26) can be used to show that for any fixed $\bar{\lambda}$ there exist arbitrarily large constant parameters a, b verifying

$$\frac{1}{n} < \frac{a}{b}\bar{\lambda} < \frac{2}{n} - \frac{1}{k_c n} \tag{27}$$

$$2b\delta > \frac{\left(k_c n^3 + 1\right)\bar{\lambda}^2}{\frac{a}{b}\bar{\lambda} - \frac{1}{n}} \tag{28}$$

with $\delta = \delta_c$ and $k_c > 1$, such that for all $t \geq 0$

$$\begin{aligned} P_c &> 0 \\ P_c F(t) + F(t)^\top P_c + \bar{\lambda} P_c &< 0\,. \end{aligned}$$

Hence, using the Lyapunov function candidate in (24), it follows that

$$\begin{aligned}\dot{V}_c(t) &= \zeta(t)^\top (P_c F(t) + F(t)^\top P_c)\zeta(t) \\ &\leq -\bar{\lambda} V_c(t)\end{aligned}$$

and consequently system (23) is globally uniformly exponentially stable. We can now conclude that the forced system (19) is ISS because it is a linear system, $L(t)$ is bounded and the homogeneous equation is exponentially stable (see Ref.[27]), and thus (20) holds.

To prove inequalities (21) and (22), we introduce the *disagreement vector* $\varrho(t) = \Pi l'(t)$ and use the facts that

$$l'_i(t) - l'_j(t) = \varrho_i(t) - \varrho_j(t) \qquad i = 1, \ldots, n;\ j = 1, \ldots, n \tag{29}$$

$$\|\varrho(t)\| = \|\zeta_1(t)\| \tag{30}$$

$$\zeta_{2_i}(t) = \chi_{I_i}(t) - \frac{v_{d_1}}{l_{f_1}} \qquad i = 1, \ldots, n-1\,. \tag{31}$$

It follows from the relations (29)–(30) that

$$\left|l'_i(t) - l'_j(t)\right| = |\varrho_i(t) - \varrho_j(t)| \leq |\varrho_i(t)| + |\varrho_j(t)| \leq 2\|\varrho(t)\| = 2\|\zeta_1(t)\|\,,$$

and thus equation (20) leads to (21) with $k_3 = 2k_2$.

On the other hand, from (16), (18), and (31) one obtains

$$\begin{aligned}\dot{l}'_1(t) - \frac{v_{d_1}}{l_{f_1}} &= -a\sum_{j\in J_1}(l'_1(t) - l'_j(t)) + \varphi_1(t) \\ \dot{l}'_i(t) - \frac{v_{d_1}}{l_{f_1}} &= -a\sum_{j\in J_i}(l'_i(t) - l'_j(t)) + \zeta_{2_{i-1}} + \varphi_i(t), \qquad i = 2, \ldots, n\,,\end{aligned}$$

which, along with (20) and $|\varphi_i(t)| \leq |e_{v_i}(t)|/l_{fi}$, lead to the bound in (22) with $k_4 = (2a\,(n-1)+1)\,k_2 + \frac{1}{l_{f_i}}$. □

Next, we consider the case where the communication graph $\Gamma(t)$ may be disconnected during some interval of time or may even fail to be connected at any instant of time; however, we assume that the connectivity of the graph satisfies the following less restrictive persistency of excitation (PE)-like condition

$$\frac{1}{T}\int_t^{t+T} \bar{L}(\tau)d\tau \geq \bar{\mu}\,\mathbb{I}_{n-1}, \qquad \forall t \geq 0 \tag{32}$$

for some $T, \bar{\mu} > 0$.

Lemma 3 *Consider the coordination system (19) and suppose that the Laplacian of the graph that models the communication topology satisfies the PE condition (32) for some $\bar{\mu}$ and sufficiently small time T. Then, for any given $\bar{\lambda} > 0$, there exist sufficiently large coordinated control gains a, b such that the system (19) is ISS with respect to $e_v(t)$, and the normalized lengths $l'_i(t)$ and path-length rates $\dot{l}'_i(t)$ satisfy (21) and (22), respectively.*

Proof. We start by showing that the origin of the homogeneous equation

$$\dot{\zeta}(t) = F(t)\zeta(t)$$

is exponentially stable. Let $V_c(\zeta(t)) = \zeta(t)^\top P_c \zeta(t)$, where P_c is defined to have the same structure as in (25). Then,

$$\dot{V}_c(t) = \zeta(t)^\top (P_c F(t) + F(t)^\top P_c)\zeta(t)$$

and therefore for any $t \geq 0$ we have

$$V_c(t+T) - V_c(t) = \int_t^{t+T} \zeta(\tau)^\top \left(P_c F(\tau) + F(\tau)^\top P_c\right)\zeta(\tau)d\tau\,.$$

Furthermore, let $\delta_{\bar{c}}$ be an arbitrary positive constant satisfying the condition

$$\delta_{\bar{c}} \;<\; \frac{1}{4}\frac{\beta}{\beta+1}\bar{\mu} \tag{33}$$

with some $\beta > 1$.

If we now set $\delta = \delta_{\bar{c}}$ in the definition of P_c, then, it can be shown that for any fixed $\bar{\lambda}$ there exist arbitrarily large constant parameters a, b verifying conditions (27)-(28) with $\delta = \delta_{\bar{c}}$ and $k_c > 2$, such that for all $t \geq 0$

$$P_c \;>\; 0\,,$$

and the following inequality holds

$$\begin{aligned} V_c(t+T) \;-\; V_c(t) \;&\leq\; \int_t^{t+T} \zeta(\tau)^\top \left(P_c F(\tau) + F(\tau)^\top P_c \;+\; \bar{\lambda} P_c\right)\zeta(\tau)d\tau \\ &\leq\; -\int_t^{t+T} 2a\zeta_1^\top(\tau)\bar{L}(\tau)\zeta_1(\tau)d\tau \;+\; \int_t^{t+T} 2a\delta_{\bar{c}}\left\|\zeta_1(\tau)\right\|^2 d\tau \;-\; \int_t^{t+T} \frac{\delta_{\bar{c}}}{\bar{\lambda}k_c n^3}\left\|\zeta_2(\tau)\right\|^2 d\tau \\ &=\; -\int_t^{t+T} 2a\left\|\bar{M}(\tau)\zeta_1(\tau)\right\|^2 d\tau \;+\; \int_t^{t+T} 2a\delta_{\bar{c}}\left\|\zeta_1(\tau)\right\|^2 d\tau \;-\; \int_t^{t+T} \frac{\delta_{\bar{c}}}{\bar{\lambda}k_c n^3}\left\|\zeta_2(\tau)\right\|^2 d\tau \end{aligned} \tag{34}$$

where $\bar{M}(t)$ is such that $\bar{L}(t) = \bar{M}^\top(t)\bar{M}(t)$. We now analyze each right hand-side term of equation (34). Using the PE condition (32), it can be concluded that

$$\frac{1}{T}\int_t^{t+T} \left\|\bar{M}(\tau)x\right\|^2 \;\geq\; \bar{\mu}\left\|x\right\|^2, \qquad \forall t \geq 0\,;\;\; \forall x \in \mathbb{R}^{n-1}\,.$$

From this, the dynamics of the coordination system (19), and using the relations

$$\begin{aligned} \left\|\zeta_1(\tau)\right\|^2 \;&\geq\; \frac{1}{2}\|\zeta_1(t)\|^2 - \|\zeta_1(\tau)-\zeta_1(t)\|^2 \\ \left\|\zeta_2(\tau)\right\|^2 \;&\geq\; \frac{1}{2}\|\zeta_2(t)\|^2 - \|\zeta_2(\tau)-\zeta_2(t)\|^2\,, \end{aligned}$$

it can be proved that the following inequalities hold

$$\begin{aligned} \int_t^{t+T}\left\|\bar{M}(\tau)\zeta_1(\tau)\right\|^2 d\tau \;&\geq\; \frac{1}{2}\int_t^{t+T}\left\|\bar{M}(\tau)\zeta_1(t)\right\|^2 d\tau \;-\; \int_t^{t+T}\left\|\bar{M}(\tau)(\zeta_1(\tau)-\zeta_1(t))\right\|^2 d\tau \\ &\geq\; \frac{1}{2}\bar{\mu}T\left\|\zeta_1(t)\right\|^2 \;-\; a^2M^4T^2\int_t^{t+T}\left\|\bar{M}(\tau)\zeta_1(\tau)\right\|^2 d\tau \;-\; M^2T^2\int_t^{t+T}\left\|\zeta_2(\tau)\right\|^2 d\tau \end{aligned} \tag{35}$$

$$\begin{aligned} \int_t^{t+T}\left\|\zeta_1(\tau)\right\|^2 d\tau \;&\leq\; 2\int_t^{t+T}\|\zeta_1(t)\|^2 d\tau \;+\; 2\int_t^{t+T}\|\zeta_1(\tau)-\zeta_1(t)\|^2 d\tau \\ &\leq\; 2T\left\|\zeta_1(t)\right\|^2 \;+\; 2a^2M^2T^2\int_t^{t+T}\left\|\bar{M}(\tau)\zeta_1(\tau)\right\|^2 d\tau \;+\; 2T^2\int_t^{t+T}\left\|\zeta_2(\tau)\right\|^2 d\tau \end{aligned} \tag{36}$$

$$\begin{aligned} \int_t^{t+T}\left\|\zeta_2(\tau)\right\|^2 d\tau \;&\geq\; \frac{1}{2}\int_t^{t+T}\|\zeta_2(t)\|^2 d\tau \;-\; \int_t^{t+T}\|\zeta_2(\tau)-\zeta_2(t)\|^2 d\tau \\ &\geq\; \frac{T}{2}\left\|\zeta_2(t)\right\|^2 \;-\; \frac{b^2M^2T^2}{2}\int_t^{t+T}\left\|\bar{M}(\tau)\zeta_1(\tau)\right\|^2 d\tau\,, \end{aligned} \tag{37}$$

where $M > \bar{M}(t)$.

Thus, substituting (35), (36) and (37) into (34) yields

$$V_c(t+T) - V_c(t) \leq -\alpha_1 \|\zeta_1(t)\|^2 - \alpha_2 \|\zeta_2(t)\|^2 - \varepsilon_1 \int_t^{t+T} \left\|\bar{M}(\tau)\zeta_1(\tau)\right\|^2 d\tau - \varepsilon_2 \int_t^{t+T} \|\zeta_2(\tau)\|^2 d\tau$$
$$+\frac{1}{\beta}\left(\int_t^{t+T} 2a \left\|\bar{M}(\tau)\zeta_1(\tau)\right\|^2 d\tau + \int_t^{t+T} 2a\delta_{\bar{c}} \|\zeta_1(\tau)\|^2 d\tau - \int_t^{t+T} \frac{\delta_{\bar{c}}}{\bar{\lambda} k_c n^3} \|\zeta_2(\tau)\|^2 d\tau \right),$$

where $\beta > 1$ was introduced in (33) and

$$\begin{aligned}
\alpha_1 &= a\bar{\mu}T - 4\frac{\beta+1}{\beta} a\delta_{\bar{c}} T \\
\alpha_2 &= \frac{1}{2}\frac{\delta_{\bar{c}}}{\bar{\lambda} k_c n^3} T \\
\varepsilon_1 &= \frac{2a}{\beta} - \left(2a^3M^4 + 4\frac{\beta+1}{\beta}\delta_{\bar{c}} a^3 M^2 + \frac{1}{2}\frac{\delta_{\bar{c}}}{\bar{\lambda} k_c n^3} b^2 M^2\right) T^2 \\
\varepsilon_2 &= \frac{1}{\beta}\frac{\delta_{\bar{c}}}{\bar{\lambda} k_c n^3} - \left(2aM^2 + 4\frac{\beta+1}{\beta}\delta_{\bar{c}} a + \frac{1}{2}\frac{\delta_{\bar{c}}}{\bar{\lambda} k_c n^3} b^2 M^2\right) T^2 .
\end{aligned}$$

It is easy to check that condition (33) leads to $\alpha_1 > 0$. For sufficiently small time T, it follows that ε_1, $\varepsilon_2 > 0$, and then one can write

$$V_c(t+T) - V_c(t) \leq -\alpha_1 \|\zeta_1(t)\|^2 - \alpha_2 \|\zeta_2(t)\|^2 - \frac{1}{\beta}\left(V_c(t+T) - V_c(t)\right),$$

where we have used inequality (34).

Consequently, for any $t \geq 0$, we have

$$V_c(t+T) - V_c(t) \leq -\frac{\beta}{\beta+1}\left(\alpha_1 \|\zeta_1(t)\|^2 + \alpha_2 \|\zeta_2(t)\|^2\right),$$

and therefore there exists $\bar{\alpha}$, satisfying $0 < \bar{\alpha} < 1$, such that

$$V_c(t+T) - V_c(t) \leq -\bar{\alpha} V_c(t).$$

We can thus conclude that

$$V_c(t+T) \leq (1-\bar{\alpha})\, V_c(t) \leq \alpha V_c(t) \tag{38}$$

where the constant α satisfies $0 < \alpha < 1$. Applying now (38) successively we obtain for $t = (k-1)T$

$$V_c(t) \leq V_c(kT) \leq \alpha^k V_c(0), \qquad \forall t \geq kT, \quad k = 0, 1, \ldots$$

Thus, $V_c(t)$ and consequently $\zeta(t)$ converge exponentially fast to zero as $t \to \infty$. From this and the fact that the forced system (23) is linear and $L(t)$ is bounded, it follows that the ISS bound (20) holds (see Ref.[27]). Then, inequalities (21) and (22) also hold. □

Remark 2 *The PE condition (32) only requires the graph be connected in an integral sense, not pointwise in time. Similar type of conditions for other coordination laws can be found in e.g. Ref.[28] and Ref.[29].*

IV. $\mathcal{L}_1$ Adaptive Augmentation of Commercial Autopilots

So far, both the path following and time-critical coordination strategies were based on vehicle kinematics only (outer-loop control). In this set-up, the pitch and yaw rate inputs $q_c(t)$ and $r_c(t)$ were selected so as to meet the path following objectives, while the speed $v_c(t)$ was computed to achieve coordination. It is now necessary to bring the UAV dynamics into play. To this effect, the above variables must be viewed

as commands to be tracked by appropriately designed inner-loop control systems. At this point, a key constraint is included: the inner-loop control systems should build naturally on existent autopilots. Since commercial autopilots are normally designed to track simple way-point commands, we modify the pitch and yaw rates, as well as the speed commands computed before by including an $\mathcal{L}_1$ adaptive loop to ensure that the closed-loop UAV with the autopilot tracks the commands $v_c(t)$, $q_c(t)$, and $r_c(t)$ generated by the time-coordination algorithm and the path following algorithm. The main benefit of the $\mathcal{L}_1$ adaptive controller is its ability of fast and robust adaptation, which leads to desired transient performance for the system's both input and output signals simultaneously, in addition to steady-state tracking. Moreover, analytically computable performance bounds can be derived for the system output as compared to the response of a desired model, which is designed to meet the desired specifications[30–32] .

First, we consider the system $\mathcal{G}_p$, which models the closed-loop system of the UAV with the autopilot:

$$\mathcal{G}_p: \quad y(s) \quad = \quad G_p(s)(u(s)+z(s)),$$

where $G_p(s)$ is an unknown strictly proper matrix transfer function, $y(s)$ and $u(s)$ are the Laplace transforms of $y(t)$ and $u(t)$ respectively, and $z(s)$ is the Laplace transform of $z(t)$, which models unknown bounded time-varying disturbances. The system $\mathcal{G}_p$ has the input $u(t) = [v_{ad}(t)\ q_{ad}(t)\ r_{ad}(t)]^\top$ issued from the $\mathcal{L}_1$ adaptive augmentation and output $y(t) = [v(t)\ q(t)\ r(t)]^\top$.

In this paper, $G_p(s)$ is assumed to have the (decoupled) form

$$\mathcal{G}_p \quad : \quad \begin{cases} v(s) = G_v(s)\,(v_{ad}(s) + z_v(s)) \\ q(s) = G_q(s)\,(q_{ad}(s) + z_q(s)) \\ r(s) = G_r(s)\,(r_{ad}(s) + z_r(s)) \end{cases} \tag{39}$$

where $G_v(s)$, $G_q(s)$, $G_r(s)$ are unknown strictly proper and stable transfer functions, and $z_v(s)$, $z_q(s)$, $z_r(s)$ represent the Laplace transformations of the time-varying disturbance signals $z_v(t)$, $z_q(t)$ and $z_r(t)$, respectively. We note that the autopilot is designed to ensure that $y(t)$ tracks any smooth $u(t)$. We further assume that the time-varying disturbances are bounded functions of time with uniformly bounded derivatives:

$$\begin{aligned} |z_v(t)| &\le L_{v0}\,, & |\dot{z}_v(t)| &\le L_{v1} \\ |z_q(t)| &\le L_{q0}\,, & |\dot{z}_q(t)| &\le L_{q1} \\ |z_r(t)| &\le L_{r0}\,, & |\dot{z}_r(t)| &\le L_{r1} \end{aligned}$$

where L_{v0}, L_{v1}, L_{q0}, L_{q1}, L_{r0}, and L_{r1} are some conservative known bounds.

We note that only very limited knowledge of the autopilot is assumed at this point. We do not assume knowledge of the state dimension of the unknown transfer functions $G_v(s)$, $G_q(s)$ and $G_r(s)$. We only assume that these are strictly proper and stable transfer functions. This will make the resulting inner-outer control systems applicable to a wide range of aircraft. We nevertheless notice that the bandwidth of the control channel of the closed-loop UAV with the autopilot is very limited, and the model (39) is valid only for low-frequency approximation of $\mathcal{G}_p$.

Then, since $q_c(t)$ and $r_c(t)$ defined in (8)-(9) stabilize the subsystem $\mathcal{G}_e$, and $v_c(t)$ in (15) (with the coordination control algorithm (16)-(17)) leads to coordination in time, the control objective for the subsystem $\mathcal{G}_p$ is reduced to designing an adaptive output feedback controller $u(t) = [v_{ad}(t)\ q_{ad}(t)\ r_{ad}(t)]^\top$ such that the output $y(t) = [v(t)\ q(t)\ r(t)]^\top$ tracks the reference input $y_c(t) = [v_c(t)\ q_c(t)\ r_c(t)]^\top$ following a desired reference model $M(s)$, i.e.

$$\begin{aligned} v(s) &\approx M(s)v_c(s) \\ q(s) &\approx M(s)q_c(s) \\ r(s) &\approx M(s)r_c(s)\,, \end{aligned}$$

where $M(s)$ is designed to meet the desired specifications. In this paper, for simplicity, we consider a first order system, by setting

$$M(s) \quad = \quad \frac{m}{s+m}\,, \qquad m > 0\,.$$

Finally, we notice that the $\mathcal{L}_1$ adaptive augmentation presented in this section is what allows us to account for the UAV dynamics.

In the following sections, we present the $\mathcal{L}_1$ adaptive augmentation architecture for the inner-loop (see Figure 3), and state a computable uniform performance bound for the tracking error between the output of the adaptive closed-loop system and the reference input signal. We refer to Ref.[25] for a detailed derivation and discussion of this bound. Since the systems in (39) have the same structure, we will define the $\mathcal{L}_1$ adaptive control architecture only for the system $G_q(s)$. The same analysis can be applied to the systems $G_v(s)$ and $G_r(s)$. The stability of the cascaded coordinated path following closed-loop system with the $\mathcal{L}_1$ adaptive augmentation will be proven in Sections V and VI.

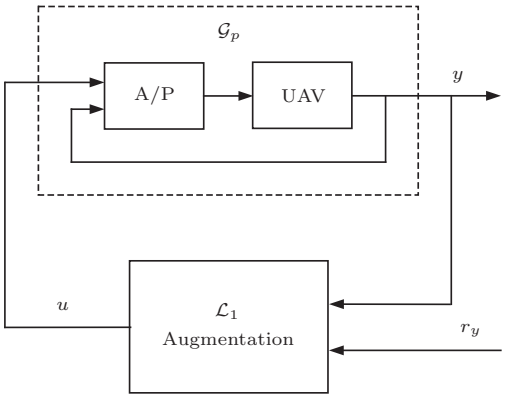

Figure 3. Inner loop structure with the $\mathcal{L}_1$ adaptive augmentation

IV.A. $\mathcal{L}_1$ Adaptive Output Feedback Controller

We notice that the system

$$q(s) = G_q(s)\left(q_{ad}(s) + z_q(s)\right) \tag{40}$$

can be rewritten in terms of the desired system behavior, defined by $M(s)$, as

$$q(s) = M(s)\left(q_{ad}(s) + \sigma_q(s)\right), \tag{41}$$

where the uncertainties due to $G_q(s)$ and $z_q(s)$ are lumped in the signal $\sigma_q(s)$, which is defined as

$$\sigma_q(s) = \frac{\left(G_q(s) - M(s)\right) q_{ad}(s) + G_q(s) z_q(s)}{M(s)}. \tag{42}$$

The philosophy of the $\mathcal{L}_1$ adaptive output feedback controller is to obtain an estimate of the unknown signal $\sigma_q(t)$, and define a *control signal* which compensates for these uncertainties within the bandwidth of a low-pass filter $C(s)$ introduced in the feedback loop. This filter guarantees that the $\mathcal{L}_1$ adaptive controller stays in the low-frequency range even in the presence of high adaptive gains and large reference inputs. The choice of $C(s)$ defines the trade-off between performance and robustness[32]. *Adaptation* is based on the projection operator, ensuring boundedness of the adaptive parameters by definition[33], and uses the output of a *state predictor* to update the estimate of $\sigma_q(t)$. This state predictor is defined to have the same structure of the open-loop system (41), using the estimate of $\sigma_q(t)$ instead of $\sigma_q(t)$ itself, which is unknown. The $\mathcal{L}_1$ adaptive control architecture for the pitch-rate channel is represented in Figure 4 and its elements are introduced below.

State Predictor: We consider the state predictor

$$\dot{\hat{q}}(t) = -m\hat{q}(t) + m\left(q_{ad}(t) + \hat{\sigma}_q(t)\right), \quad \hat{q}(0) = q(0), \tag{43}$$

where the adaptive estimate $\hat{\sigma}_q(t)$ is governed by the following adaptation law.

Adaptive Law: The adaptation of $\hat{\sigma}_q(t)$ is defined as

$$\dot{\hat{\sigma}}_q(t) = \Gamma_c \mathrm{Proj}(\hat{\sigma}_q(t), -\tilde{q}(t)), \ \hat{\sigma}_q(0) = 0, \tag{44}$$

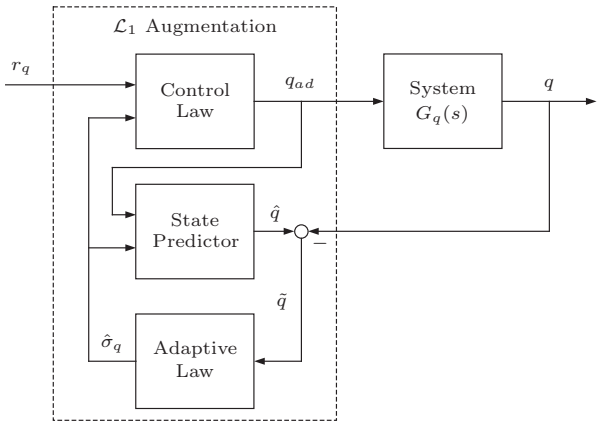

Figure 4. $\mathcal{L}_1$ adaptive augmentation loop for pitch rate control

where $\tilde{q}(t) = \hat{q}(t) - q(t)$ is the error signal between the state predictor in (43) and the output of the system in (40), $\Gamma_c \in \mathbb{R}^+$ is the adaptation rate subject to a computable lower bound, and Proj denotes the projection operator.

Control Law: The control signal is generated by

$$q_{ad}(s) \quad = \quad C(s)\left(r_q(s) - \hat{\sigma}_q(s)\right), \tag{45}$$

where $r_q(t)$ is a bounded reference input signal with bounded derivative, and $C(s)$ is a strictly proper low-pass filer with $C(0) = 1$. In this paper, we consider the simplest choice of a first order filter

$$C(s) \quad = \quad \frac{\omega}{s+\omega}, \qquad \omega > 0\,.$$

The complete $\mathcal{L}_1$ adaptive output feedback controller consists of (43), (44) and (45) subject to the following stability condition: the design of $C(s)$ and $M(s)$ needs to ensure that

$$H(s) \quad = \quad \frac{G_q(s)M(s)}{C(s)G_q(s) + (1 - C(s))M(s)} \tag{46}$$

is stable[b].

IV.B. Analysis of the $\mathcal{L}_1$ Adaptive Controller

In this section we discuss the stability of the closed-loop adaptive system and the performance bound for system's output with respect to the reference command. We avail ourselves of previous work on $\mathcal{L}_1$ augmentation and its application to path following[25,34].

Lemma 4 *Let $r_q(t)$ be a bounded reference command with bounded derivative. Given the $\mathcal{L}_1$ adaptive controller defined via (43), (44) and (45) subject to (46), if the adaptation gain Γ_c and the projection bounds are appropriately chosen[c] and, moreover, the initial conditions satisfy*

$$|q(0) - r_q(0)| \quad \leq \quad \frac{\gamma_{\dot{r}_q}}{m},$$

where $\gamma_{\dot{r}_q}$ is the bound on the derivative of $r_q(t)$, then we have

$$\|q - r_q\|_{\mathcal{L}_\infty} \quad \leq \quad \gamma_\theta \tag{47}$$

where $\gamma_\theta = \gamma_q + \bar{\gamma}_q + \frac{\gamma_{\dot{r}_q}}{m}$ and, moreover, $\lim_{\Gamma_c \to \infty}\left(\gamma_q + \lim_{\omega \to \infty} \bar{\gamma}_q\right) = 0$.

[b]This stability condition is a simplified version of the original condition derived in Ref.[34], where the problem formulation includes output dependent disturbance signals $z(t) = f(t, y(t))$.

[c]See Ref.[25] for a detailed discussion and derivation of the design constraints on the adaptation gain Γ_c, the bandwidth of the low-pass filter ω, and the bandwidth of the state-predictor m.

Proof. The proof of this Lemma can be found in Ref.[25] . □

Similarly, if we implement the $\mathcal{L}_1$ adaptive controller for the systems

$$\begin{aligned} v(s) &= G_v(s)\left(v_{ad}(s)+z_v(s)\right) \\ r(s) &= G_r(s)\left(r_{ad}(s)+z_r(s)\right) \end{aligned}$$

subject to

$$\begin{aligned} |v(0)-v_c(0)| &\leq \frac{\|\dot{v}_c\|_{\mathcal{L}_\infty}}{m}, \\ |r(0)-r_c(0)| &\leq \frac{\|\dot{r}_c\|_{\mathcal{L}_\infty}}{m}, \end{aligned}$$

we can derive

$$\|v-v_c\|_{\mathcal{L}_\infty} \leq \gamma_v \tag{48}$$

$$\|r-r_c\|_{\mathcal{L}_\infty} \leq \gamma_\psi \tag{49}$$

with $\gamma_v > 0$ and $\gamma_\psi > 0$ being constants similar to γ_θ. We note that γ_v, γ_θ, and γ_ψ can be rendered arbitrarily small by increasing the adaptation gain Γ_c, the bandwidth of the low-pass filter ω, and the bandwidth of the state predictor m.

Remark 3 *We note that the derivation of the performance bounds with the $\mathcal{L}_1$ adaptive augmentation assumes bounded reference commands with bounded derivatives, and thus before using these performance bounds one should make sure that these conditions are satisfied.*

V. Path Following with $\mathcal{L}_1$ Adaptive Augmentation

At this point, we discuss the stability of the path following closed-loop system with the $\mathcal{L}_1$ augmentation for a single UAV (see Figure 5). First, we need to show that the outer-loop path following commands $q_c(t)$ and $r_c(t)$ and their derivatives $\dot{q}_c(t)$ and $\dot{r}_c(t)$ are bounded, which in turn allows us to prove that the original domain of attraction for the kinematic error equations given in (10) can be retained with the $\mathcal{L}_1$ augmentation.

Lemma 5 *If $x(t) \in \bar{\Omega}$ for all $t \geq 0$, where $\bar{\Omega}$ is the closure of the set Ω, which was defined in (10), and the UAV speed $v(t)$ is upper bounded (that is, $v(t) \leq v_{\max}$), then there exist control parameters Γ_c, ω and m such that the outer-loop path following commands $q_c(t)$ and $r_c(t)$ and their derivatives $\dot{q}_c(t)$ and $\dot{r}_c(t)$ are bounded, that is*

$$\begin{aligned} \|q_c\|_{\mathcal{L}_\infty} &\leq \gamma_{q_c}, & \|\dot{q}_c\|_{\mathcal{L}_\infty} &\leq \gamma_{\dot{q}_c} \\ \|r_c\|_{\mathcal{L}_\infty} &\leq \gamma_{r_c}, & \|\dot{r}_c\|_{\mathcal{L}_\infty} &\leq \gamma_{\dot{r}_c}, \end{aligned} \tag{50}$$

for some positive constants γ_{q_c}, $\gamma_{\dot{q}_c}$, γ_{r_c}, and $\gamma_{\dot{r}_c}$.

Proof. The proof of this Lemma can be found in Ref.[25] . □

Now, we define $u_\theta(t)$ and $u_\psi(t)$ as

$$\begin{bmatrix} u_\theta(t) \\ u_\psi(t) \end{bmatrix} = D\left(t,\theta_e\psi_e\right) + T\left(t,\theta_e\right) \begin{bmatrix} q(t) \\ r(t) \end{bmatrix}, \tag{51}$$

and therefore, from (1), one gets

$$\begin{aligned} \dot{\theta}_e(t) &= u_\theta(t) \\ \dot{\psi}_e(t) &= u_\psi(t). \end{aligned}$$

Then, it follows from (8) and (51) that

$$\begin{bmatrix} u_\theta(t)-u_{\theta_c}(t) \\ u_\psi(t)-u_{\psi_c}(t) \end{bmatrix} = T\left(t,\theta_e\right) \begin{bmatrix} q(t)-q_c(t) \\ r(t)-r_c(t) \end{bmatrix}. \tag{52}$$

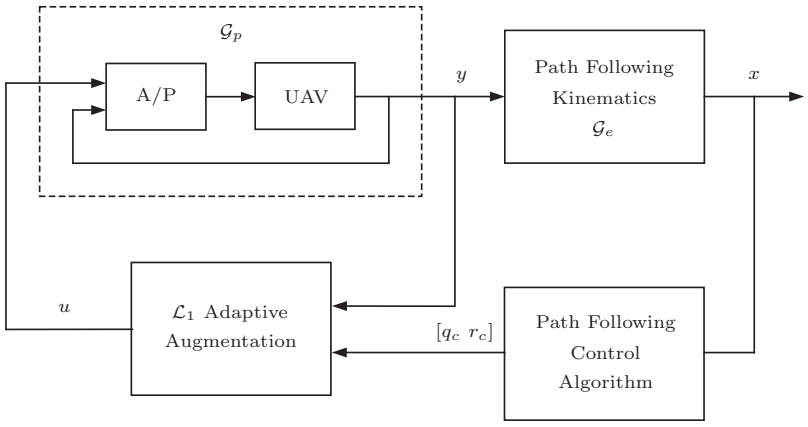

Figure 5. Path following closed-loop system for a single UAV with $\mathcal{L}_1$ adaptive augmentation

Furthermore, we define γ_{u_θ} and γ_{u_ψ} as

$$\begin{aligned} \gamma_{u_\theta} &= \sqrt{\gamma_\theta^2 + \gamma_\psi^2} \\ \gamma_{u_\psi} &= \frac{1}{\cos\nu_1}\sqrt{\gamma_\theta^2 + \gamma_\psi^2}\,, \end{aligned} \tag{53}$$

with γ_θ and γ_ψ being the bounds in (47) and (49) for $r_q(t) \equiv q_c(t)$ and $r_r(t) \equiv r_c(t)$.

Theorem 1 *Let $d = \sqrt{cc_1}$, where c and c_1 were introduced in (6), and let the progression of the point P along the path be governed by (7). For any smooth $v(t)$, verifying (5), if*

1. *the initial condition for the path following state vector satisfies*

$$x(0) \in \Omega\,,$$

where Ω was defined in (10);

2. *the initial conditions for the pitch and yaw rates are bounded as*

$$\begin{aligned} |q(0) - q_c(0)| &\leq \frac{\gamma_{\dot{q}_c}}{m} \\ |r(0) - r_c(0)| &\leq \frac{\gamma_{\dot{r}_c}}{m} \end{aligned}$$

where $\gamma_{\dot{q}_c}$ and $\gamma_{\dot{r}_c}$ were introduced in (50); and in addition

3. *Γ_c, ω, and m verify*

$$\gamma_{u_\theta} + \gamma_{u_\psi} \leq \frac{\sqrt{cc_2}}{2}\frac{\lambda_{\min}(\bar{Q}_p)}{\lambda_{\max}(P_p)}\,, \tag{54}$$

where γ_{u_θ} and γ_{u_ψ} were defined in (53),

then $x(t) \in \Omega$ for all $t \geq 0$, that is

$$V_p(x(t)) < \frac{c}{2}\,, \qquad \forall\ t \geq 0\,,$$

and the path following closed-loop cascaded system is ultimately bounded with the bounds given in (12).

Proof. The proof of this Theorem can be found in Ref.[25] . □

Remark 4 *We notice that this approach is different from common backstepping-type analysis for cascaded systems. The advantage of the above structure for the feedback design is that it retains the properties of the autopilot, which is designed to stabilize the inner-loop. As a result, it leads to ultimate boundedness instead of asymptotic stability. From a practical point of view, the procedure adopted for inner/outer loop control system design is quite versatile in that it adapts itself to the particular autopilot installed on-board the UAV.*

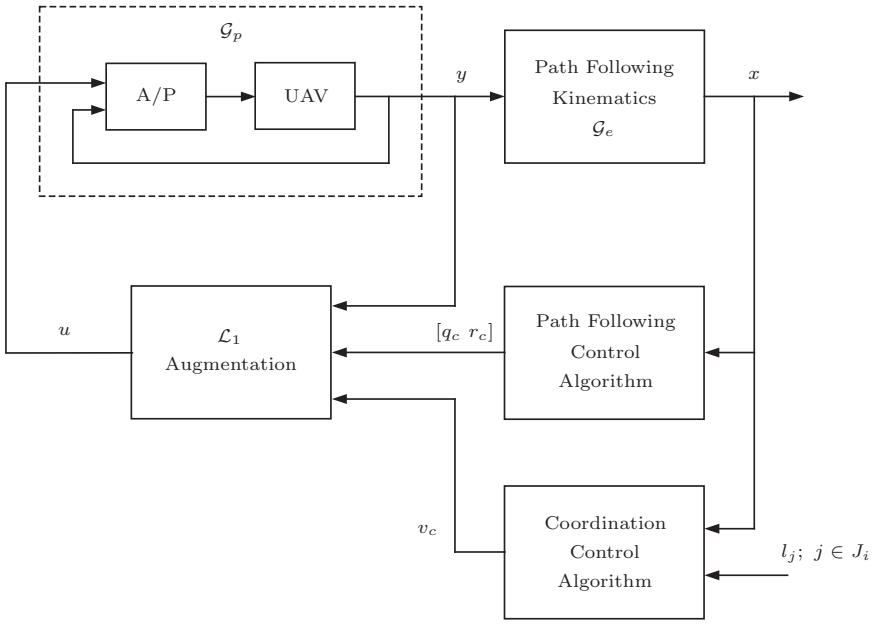

Figure 6. Coordinated path following closed-loop for the ith UAV with $\mathcal{L}_1$ augmentation

VI. Combined Path Following and Time-Critical Coordination with $\mathcal{L}_1$ Adaptive Augmentation

This section addresses the stability properties of the combined coordination/path following systems and the inner-loop with $\mathcal{L}_1$ adaptive augmentation. The complete coordinated path following closed-loop system for a single UAV is presented in Figure 6. The main result is stated in Theorem 2. First, however, we need to show that the outer-loop reference commands $v_c(t)$, $q_c(t)$, and $r_c(t)$ and their derivatives are bounded.

Lemma 6 *If $x(t) \in \bar{\Omega}$ for all $t \geq 0$, and the the initial conditions and the design of the $\mathcal{L}_1$ adaptive augmentation verify the following relations*

$$\begin{aligned} |v(0) - v_c(0)| &\leq \frac{\gamma_{\dot{v}_c}}{m} \\ \left|v(t_s^+) - v_c(t_s^+)\right| &\leq \frac{\gamma_{\dot{v}_c}}{m} \\ \bar{\bar{k}}_1 \left\|\zeta(0)\right\| &< \frac{(v_{\max} - \bar{\gamma}_v)\cos\nu_1 \cos\nu_2 - K_1 d}{l_{f_{\max}}} - \frac{v_{d_1}}{l_{f_1}} - \bar{\bar{k}}_2 \bar{\gamma}_v \,, \end{aligned} \tag{55}$$

where t_s are the times at which the communication topology switches, $\bar{\gamma}_v = \max\{\gamma_{v_1}, \ldots, \gamma_{v_n}\}$, $l_{f_{\max}} = \max\{l_{f_1}, \ldots, l_{f_n}\}$ and some $\bar{\bar{k}}_1, \bar{\bar{k}}_2 > 0$, then the coordination/path following outer-loop commands $v_c(t)$, $q_c(t)$ and $r_c(t)$ and their derivatives $\dot{v}_c(t)$, $\dot{q}_c(t)$ and $\dot{r}_c(t)$ are bounded, that is

$$\begin{aligned} \|v_c\|_{\mathcal{L}_\infty} &\leq \gamma_{v_c} \,, & \|\dot{v}_c\|_{\mathcal{L}_\infty} &\leq \gamma_{\dot{v}_c} \\ \|q_c\|_{\mathcal{L}_\infty} &\leq \gamma_{q_c} \,, & \|\dot{q}_c\|_{\mathcal{L}_\infty} &\leq \gamma_{\dot{q}_c} \\ \|r_c\|_{\mathcal{L}_\infty} &\leq \gamma_{r_c} \,, & \|\dot{r}_c\|_{\mathcal{L}_\infty} &\leq \gamma_{\dot{r}_c} \,, \end{aligned} \tag{56}$$

with some positive constants γ_{v_c}, $\gamma_{\dot{v}_c}$, γ_{q_c}, $\gamma_{\dot{q}_c}$, γ_{r_c}, and $\gamma_{\dot{r}_c}$. Furthermore, the resulting velocity for the ith UAV verifies the a priori *specified upper bound $v_i(t) \leq v_{\max}$.*

Proof. The proof is omitted due to space limitations. □

Theorem 2 *Consider the combined path following system (1) and time-critical coordination system (19) under the communication constraints of Lemma 2 or Lemma 3. If, for every UAV, we have*

1. *the initial condition for the path following state vector satisfies*

$$x_i(0) \in \Omega\,,$$

where Ω *was defined in (10);*

2. *the initial conditions for the speed, pitch rate, and yaw rate are bounded as*

$$\begin{aligned} |v_i(0) - v_{c_i}(0)| &\leq \frac{\gamma_{\dot{v}_c}}{m} \\ |q_i(0) - q_{c_i}(0)| &\leq \frac{\gamma_{\dot{q}_c}}{m} \\ |r_i(0) - r_{c_i}(0)| &\leq \frac{\gamma_{\dot{r}_c}}{m} \\ \left|v_i(t_s^+) - v_{c_i}(t_s^+)\right| &\leq \frac{\gamma_{\dot{v}_c}}{m} \end{aligned}$$

where $\gamma_{\dot{v}_c}$, $\gamma_{\dot{q}_c}$, *and* $\gamma_{\dot{r}_c}$ *were introduced in (56); and*

3. *the control parameters* Γ_c, ω, *and* m *verify (54), (55), and also*

$$\bar{\bar{k}}_1 \left\|\zeta(0)\right\| < \frac{v_{d_1}}{l_{f_1}} - \frac{(v_{\min} + \bar{\gamma}_v) + K_1 d}{l_{f_{\min}}} - \bar{\bar{k}}_2 \bar{\gamma}_v\,, \tag{57}$$

where $l_{f_{\min}} = \min\{l_{f_1}, \ldots, l_{f_n}\}$, *and* $\bar{\gamma}_v$ *and* $\bar{\bar{k}}_1, \bar{\bar{k}}_2 > 0$ *were introduced in Lemma 6,*

then $x_i(t) \in \Omega$ *for all* $t \geq 0$ *and* $i = 1, \ldots, n$, *and the complete closed-loop cascaded system is ultimately bounded with the bounds given in (12). Moreover, the coordination error* $\zeta(t)$ *satisfy*

$$\left\|\zeta(t)\right\| \leq k_1 \left\|\zeta(0)\right\| \mathrm{e}^{-\bar{\lambda}(t)} + k_2 \bar{\gamma}_v\,, \tag{58}$$

and the resulting velocity for the i*th UAV verifies the* a priori *specified bounds* $0 < v_{\min} \leq v_i(t) \leq v_{\max}$.

Proof. Consider the ith UAV. Using the same Lyapunov function candidate $V_p(x)$ as in Lemma 1, it follows that

$$\dot{V}_{p_i} \leq -x_i^\top Q_{p_i} x_i + \frac{|\theta_{e_i} - \delta_{\theta_i}|}{c_2} |u_{\theta_i} - u_{\theta_{ci}}| + \frac{|\psi_{e_i} - \delta_{\psi_i}|}{c_2} |u_{\psi_i} - u_{\psi_{ci}}| \tag{59}$$

where Q_{p_i} was defined in (11), and we have taken into consideration the errors between $u_{\theta_i}(t)$ and $u_{\theta_{ci}}(t)$, and $u_{\psi_i}(t)$ and $u_{\psi_{ci}}(t)$ (or equivalently between $q_i(t)$ and $q_{c_i}(t)$, and $r_i(t)$ and $r_{c_i}(t)$). Next we will show that, under the conditions of the Theorem, Q_{p_i} is positive definite and the terms $|\theta_{e_i} - \delta_{\theta_i}|$, $|u_{\theta_i} - u_{\theta_{ci}}|$, $|\psi_{e_i} - \delta_{\psi_i}|$, and $|u_{\psi_i} - u_{\psi_{ci}}|$ are bounded, and thus the original domain of attraction for the kinematic error equations given in (10) can be retained.

We prove this Theorem by contradiction. Since $x_i(0) \in \Omega$ by assumption, and $V_{p_i}(t)$ is continuous and differentiable, if $x_i(t) \in \Omega \;\; \forall t \geq 0$ is not true, then there exists a time τ such that

$$\begin{aligned} V_{p_i}(t) &< \frac{c}{2}\,, \qquad \forall\, 0 \leq t < \tau \\ V_{p_i}(\tau) &= \frac{c}{2}\,, \end{aligned} \tag{60}$$

which implies

$$\dot{V}_{p_i}(\tau) > 0\,. \tag{61}$$

First, we show that the speed of the ith UAV verifies $v_i(t) > v_{\min}$ for all $t \in [0, \tau]$, which in turn will help us prove that Q_{p_i} is positive definite. It follows from Lemma 6 that the commanded reference signals $v_{c_i}(t)$, $q_{c_i}(t)$, and $r_{c_i}(t)$ and their derivatives $\dot{v}_{c_i}(t)$, $\dot{q}_{c_i}(t)$, and $\dot{r}_{c_i}(t)$ are bounded for all $t \in [0, \tau]$, i.e.

$$\begin{aligned} \left\|v_{c_i\tau}\right\|_{\mathcal{L}_\infty} &\leq \gamma_{v_c}\,, & \left\|\dot{v}_{c_i\tau}\right\|_{\mathcal{L}_\infty} &\leq \gamma_{\dot{v}_c} \\ \left\|q_{c_i\tau}\right\|_{\mathcal{L}_\infty} &\leq \gamma_{q_c}\,, & \left\|\dot{q}_{c_i\tau}\right\|_{\mathcal{L}_\infty} &\leq \gamma_{\dot{q}_c} \\ \left\|r_{c_i\tau}\right\|_{\mathcal{L}_\infty} &\leq \gamma_{r_c}\,, & \left\|\dot{r}_{c_i\tau}\right\|_{\mathcal{L}_\infty} &\leq \gamma_{\dot{r}_c}\,, \end{aligned} \tag{62}$$

and moreover one has

$$v_i(t) \quad \leq \quad v_{\max}\,, \qquad \forall t \in [0,\tau]\,.$$

Therefore, from this result and the bounds on the initial conditions in (57), one finds that the bounds in (47), (48), and (49) hold with $r_v(t) \equiv v_{c_i}(t)$, $r_q(t) \equiv q_{c_i}(t)$, $r_r(t) \equiv r_{c_i}(t)$, and for any $t \in [0,\tau]$. So we have

$$\begin{aligned} \|(v_i - v_{c_i})_\tau\|_{\mathcal{L}_\infty} &\leq \gamma_{v_i} && (63)\\ \|(q_i - q_{c_i})_\tau\|_{\mathcal{L}_\infty} &\leq \gamma_{\theta_i} && (64)\\ \|(r_i - r_{c_i})_\tau\|_{\mathcal{L}_\infty} &\leq \gamma_{\psi_i}\,. && (65) \end{aligned}$$

Using (20), similar to (22), it can be shown that

$$u_{\text{coord}_i}(t) \quad \geq \quad \frac{v_{d_1}}{l_{f_1}} - \bar{\bar{k}}_1 \|\zeta(0)\| - \bar{\bar{k}}_2 \sup_{t\in[0,\tau]} \|e_v(t)\|\,, \tag{66}$$

with $\bar{\bar{k}}_1 = (2a(n-1)+1)k_1$ and $\bar{\bar{k}}_2 = (2a(n-1)+1)k_2$. Since at any $t \in [0,\tau]$ the path following error states $x_i(t)$ lie in the compact set $\bar{\Omega}$, then

$$v_{c_i}(t) \quad \geq \quad u_{coord_i}(t) l_{f_i} - K_1 d\,,$$

and thus, applying (57), (63), and (66) to the above inequality yields

$$v_{c_i}(t) \quad > \quad v_{\min} + \bar{\gamma}_v\,.$$

Finally, since $\|e_{v_i\tau}\|_{\mathcal{L}_\infty} \leq \gamma_{v_i}$, it follows that

$$v_i(t) \;\geq\; v_{c_i}(t) - \gamma_{v_i} \quad > \; v_{\min}\,,$$

for all $t \in [0,\tau]$. This result, along with the fact that $x_i(t) \in \bar{\Omega}$ for any $t \in [0,\tau]$, leads to

$$\dot{V}_{p_i} \quad \leq \quad -x_i^\top \bar{Q}_{p_i} x_i \;+\; \frac{|\theta_{e_i} - \delta_{\theta_i}|}{c_2} |u_{\theta_i} - u_{\theta_{ci}}| \;+\; \frac{|\psi_{e_i} - \delta_{\psi_i}|}{c_2} |u_{\psi_i} - u_{\psi_{ci}}|\,, \qquad \forall t \in [0,\tau]\,,$$

where $\bar{Q}_{p_i}$ was defined in (13).

Next we show that, under the conditions of the Theorem, the terms $|\theta_{e_i} - \delta_{\theta_i}|$, $|u_{\theta_i} - u_{\theta_{ci}}|$, $|\psi_{e_i} - \delta_{\psi_i}|$, and $|u_{\psi_i} - u_{\psi_{ci}}|$ are bounded. It follows from (52) that

$$\begin{aligned} u_{\theta_i}(t) - u_{\theta_{ci}}(t) &= \cos\phi_{e_i}(t)\,(q_i(t) - q_{c_i}(t)) - \sin\phi_{e_i}(t)\,(r_i(t) - r_{c_i}(t))\\ u_{\psi_i}(t) - u_{\psi_{ci}}(t) &= \frac{\sin\phi_{e_i}(t)}{\cos\theta_{e_i}(t)}\,(q_i(t) - q_{c_i}(t)) + \frac{\cos\phi_{e_i}(t)}{\cos\theta_{e_i}(t)}\,(r_i(t) - r_{c_i}(t))\,, \end{aligned}$$

and hence, from the bounds in (64) and (65), we have

$$\begin{aligned} \|(u_{\theta_i} - u_{\theta_{ci}})_\tau\|_{\mathcal{L}_\infty} &\leq \gamma_{u_{\theta i}}\\ \|(u_{\psi_i} - u_{\psi_{ci}})_\tau\|_{\mathcal{L}_\infty} &\leq \gamma_{u_{\psi i}}\,, \end{aligned} \tag{67}$$

with $\gamma_{u_{\theta i}}$ and $\gamma_{u_{\psi i}}$ defined in (53). Moreover, it follows from (60) that for any $t \in [0,\tau]$

$$\begin{aligned} |\theta_{e_i}(t) - \delta_{\theta_i}(t)| &\leq \sqrt{cc_2}\\ |\psi_{e_i}(t) - \delta_{\psi_i}(t)| &\leq \sqrt{cc_2}\,. \end{aligned} \tag{68}$$

Therefore, from Eqs. (59), (67) and (68), one finds

$$\dot{V}_{p_i}(\tau) \quad \leq \quad -x_i^\top(\tau)\bar{Q}_{p_i} x_i(\tau) + \sqrt{\frac{c}{c_2}}(\gamma_{u_{\theta i}} + \gamma_{u_{\psi i}})\,.$$

Since

$$x_i^\top(\tau)\bar{Q}_{p_i} x(\tau) \quad \geq \quad \frac{\lambda_{\min}(\bar{Q}_{p_i})}{\lambda_{\max}(P_{p_i})} V_{p_i}(\tau)\,,$$

where $\lambda_{\min}(\bar{Q}_{p_i})$ and $\lambda_{\max}(P_{p_i})$ are the minimum and the maximum eigenvalues of $\bar{Q}_{p_i}$ and P_{p_i} respectively, it follows from (60) that

$$x_i^\top(\tau)\bar{Q}_{p_i}x_i(\tau) \quad \geq \quad \frac{c}{2}\frac{\lambda_{\min}(\bar{Q}_{p_i})}{\lambda_{\max}(P_{p_i})}\,,$$

and then the design constraint in (54) leads to

$$\dot{V}_{p_i}(\tau) \quad \leq \quad 0\,,$$

which contradicts the assumption in (61), and thus $x_i(t) \in \Omega$ holds for all $t \geq 0$ and $i = 1, \ldots, n$. Since (60) leads to (62)-(68) for any time $t \in [0, \tau]$, $x_i(t) \in \Omega$ implies that the bounds in (12) hold for all $t \geq 0$.

Finally, equations (20) and (63) lead to the bound in (58), which concludes the proof. □

VII. Experimental Results

The complete coordinated path following control system with $\mathcal{L}_1$ adaptive augmentation, shown in Figure 6, was implemented on experimental UAV RASCALs operated by NPS. The Hardware-In-The-Loop (HITL) and flight test setups[20] are shown in Figure 7; note that both configurations are identical except the sensor data is software generated in the HITL simulation.

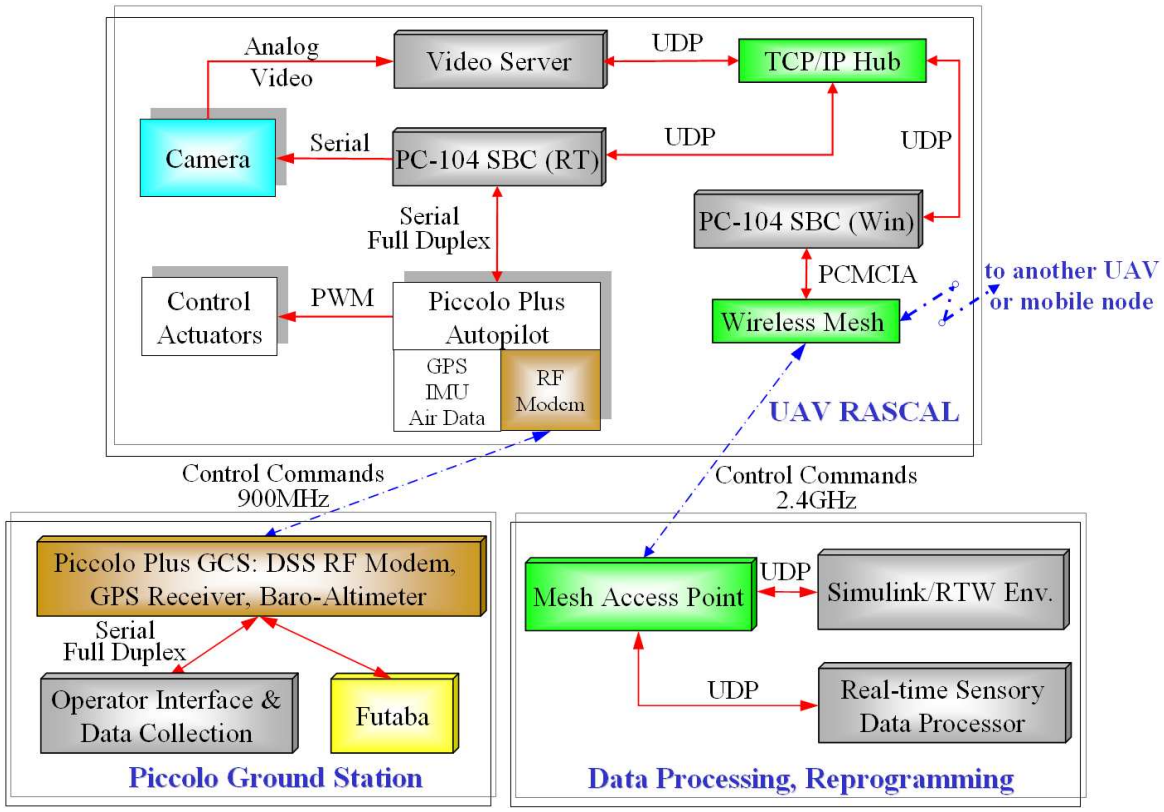

Figure 7. Avionics architecture including two embedded processors and an AP

Customized RASCAL model aircraft were used for the experimental part of the work. The payload bay of each aircraft is used to house two PC104 embedded computers assembled in a stack, wireless network link, and the Piccolo autopilot[35] with its dedicated control channel. The first PC-104 board (see SBC (RT) in Figure 7) runs developed algorithms in real-time while directly communicating with the autopilot (AP) over the serial link. The second PC-104 computer (see SBC (Win) in Figure 7) is equipped with a mesh network card (Motorola WMC6300 Mesh Card) that provides wireless communication to another UAV as well as to the data processing center on the ground. This second computer performs software bridging of onboard wired and external wireless mesh networks. Thus, direct connection with the onboard autopilot efficiently

eliminates communication delays between the high-level control algorithm and the autopilot. In turn, an integration of the self-configuring wireless mesh network allows for transparent inter-vehicle communication making it suitable for coordination in time.

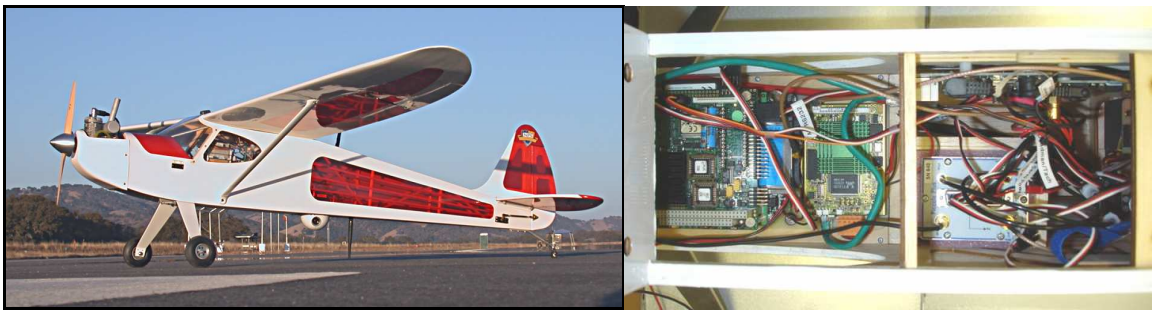

Figure 8. RASCAL UAV and its payload bay with the custom built avionics

Based on the presented hardware setup, the developed algorithm was flight tested in February 2007. Figure 9 shows how the developed system was used for the flight testing of the path following/adaptation/coordination algorithms running onboard in real-time; a collective picture of 15 trials obtained during just one flight test is presented. As for the coordination, the speed of virtual cooperative UAV was simulated to be constant. In this picture, the red trajectories represent the required/commanded flight path and the blue one shows the actual flight path of the UAV. Each trial was used to tune the control law parameters in order to achieve more accurate path following and coordination.

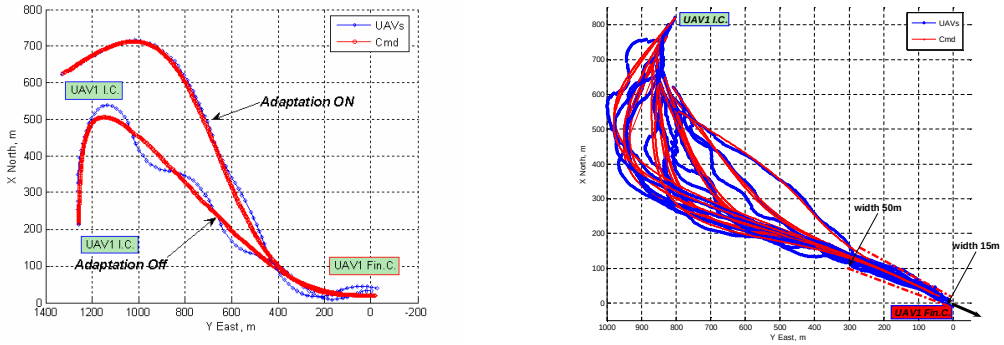

Figure 9. Performance comparison with and without $\mathcal{L}_1$ adaptation (top) and 3D path following in the autonomous landing scenario (bottom)

Figure 10(a) presents one of the trials of Figure 9 in details; it shows the inertial position of UAV with respect to the commanded feasible trajectory generated online as introduced in Section II. Figure 10(b) also shows the corresponding rate commands of the autopilot as well as errors of the UAV tracking the trajectory. It can be seen that the maximum deviation from the desired trajectory is about $40m$, which corresponds to the point of the sharp turn. Other than at this point, the tracking errors are very small and the UAV is following the commanded path very closely.

Figures 10(c)-10(d) include results of an HITL test where two UAVs follow feasible trajectories while using their velocities to coordinate simultaneous arrival at their respective terminal conditions. Results of Figure 10(c) show the desired and the actual paths of each UAV. Control commands and errors for both UAVs are similar to the results of one UAV tracking the path. As in the case of one UAV, the control efforts required to bring each airplane to the commanded trajectory do not exceed any limitations imposed by the autopilot and are typical for this class of UAVs. Finally, normalized coordination states for each UAV are presented in Figure 10(d); two graphs represent coordination efforts required to deliver two UAVs to the terminal conditions at the same time. Both airplanes arrive at the final position at nearly the same time.

The results presented above demonstrate feasibility of the onboard integration of the path following, adaptation and coordination concepts. During the flight experiments, the required control commands (including adaptive contribution) have never exceeded the limits defined for the UAV in traditional waypoint navigation mode. At the same time the achieved functionality of the UAV following 3D curves in inertial

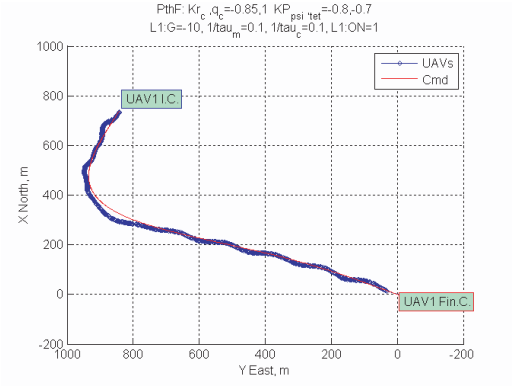

(a) Desired (red) and actual (blue) UAV trajectories from flight test with $\mathcal{L}_1$ adaptive controller

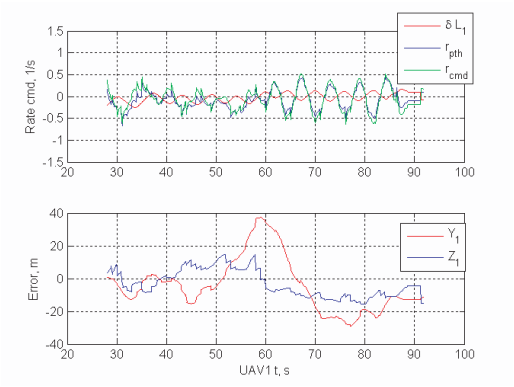

(b) Top: path following turn rate command and contributions from outer loop and $\mathcal{L}_1$ adaptation. Bottom: path following errors

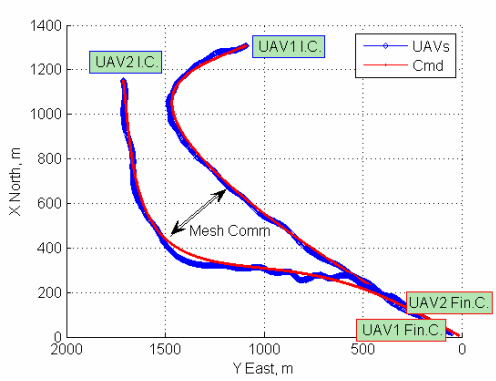

(c) Simultaneous arrival of two UAVs to the same terminal conditions (separated by altitude).

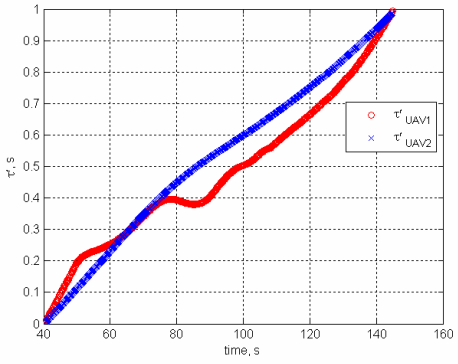

(d) Coordination states for each UAV.

Figure 10. Flight Test Results (top) and Hardware-in-the-Loop Simulations (bottom)

space has never been available for the airplanes equipped with traditional AP; adaptive concept explicitly outperforms the conventional waypoint navigation method. Presented results not only demonstrate the feasibility of the concept but provide a roadmap for further development and onboard implementation of intelligent multi-UAV coordination.

VIII. Conclusion

This paper presented a solution to the problem of coordinated path following control of multiple unmanned air vehicles (UAVs) in the presence of time-varying communication topologies with the objective of meeting desired spatial and/or temporal constraints. As a motivating example, a scenario was considered where a fleet of UAVs must follow spatially deconflicted paths and arrive at their final destinations at identical times. The theoretical framework adopted led to a novel methodology for coordinated motion control that brings together algorithms for path following and vehicle coordination with an inner-outer (that is, kinematic versus dynamic) structure with $\mathcal{L}_1$ adaptation. This is in striking contrast with other algorithms proposed in the literature that yield control laws which are hard to tune and do not exploit the fact that many autonomous vehicles are naturally equipped with local, highly performing dynamic control loops (autopilots).

Central to the development of the control laws derived was the combination of nonlinear path following algorithms, derived at the kinematic level, with an $\mathcal{L}_1$ adaptive output feedback control law that effectively augments an existing autopilot and yields an inner-outer loop control structure with guaranteed performance. The same principle was used at the coordination level, where multiple vehicle coordination laws that generate desired speed profiles for the vehicles in response to data exchanged over a dynamically changing

communication are complemented with inner speed control loops that are designed by resorting to $\mathcal{L}_1$ adaptive control techniques. From a theoretical standpoint, the paper offered a complete analysis of the stability properties of the Combined Path Following and Time-Critical Coordination with $\mathcal{L}_1$ Adaptive Augmentation under time-varying communication constraints. In particular, tools were developed to address explicitly the case where the communication graph that captures the underlying communication network topology may be disconnected during some interval of time or may even fail to be connected at any instant of time. Flight tests and hardware-in-the-loop simulations have shown clearly what steps are required to transition from theory to practice. The results obtained show that the methodology proposed holds considerable promise for coordinated motion control of multiple UAVs.

References

[1]I. Kaminer, A. Pascoal, E. Hallberg, and C. Silvestre. Trajectory tracking for autonomous vehicles: An integrated approach to guidance and control. *AIAA Journal of Guidance, Control, and Dynamics*, 21(1), 1998.

[2]Y. Kim and M. Mesbahi. On maximizing the second smallest eigenvalue of state-dependent graph Laplacian. *IEEE Trans. on Autom. Cont.*, 51(1):116–120, 2006.

[3]J. Tsitsiklis and M. Athans. Convergence and asymptotic agreement in distributed decision problems. *IEEE Transaction on Autom. Cont.*, 29(1):42–50, 1984.

[4]R. Sepulchre, D. Paley, and N. Leonard. Collective motion and oscillator synchronization. In *Proc. of Block Island Workshop on Cooperative Control*, pages 189–205, Block Island, RI, 2003.

[5]A. Jadbabaie, J. Lin, and A. Morse. Coordination of groups of mobile autonomous agents using nearest neighbor rules. *IEEE Trans. on Autom. Cont.*, 48(6):988–1001, 2003.

[6]Z. Lin, B. Francis, and M. Maggiore. State agreement for coupled nonlinear systems with time-varying interaction. *SIAM Journal of Control and Optimization*, 2005. in review.

[7]M. Egerstedt and X. Hu. Formation control with virtual leaders and reduced communications. *IEEE Trans. on Robotics and Automation*, 17(6):947–951, Dec. 2001.

[8]R. Ghabcheloo, A. Pascoal, C. Silvestre, and I. Kaminer. Coordinated path following control of multiple wheeled robots using linearization techniques. *International Journal of Systems Science, Taylor and Francis*, 37(6):399–414, 2006.

[9]L. Fang, P. Antsaklis, and A. Tzimas. Asynchronous consensus protocols: Preliminary results, simulations and open questions. In *Proc. of IEEE Conf. on Decision and Control*, pages 2194–2199, Seville, Spain, 2005.

[10]M. Mesbahi. On state-dependent dynamic graphs and their controllability properties. *IEEE Trans. on Autom. Cont.*, 50(3):387–392, 2005.

[11]D. Stilwell and B. Bishop. Platoons of underwater vehicles. *IEEE Control Systems Magazine*, 20(6):45–52, Dec. 2000.

[12]D. Stilwell, E. Bollt, and D. Roberson. Sufficient conditions for fast switching synchronization in time-varying network topologies. *SIAM Journal of Applied Dynamical Systems*, 6(1):140–156, 2006.

[13]M. Cao, D. Spielman, and A. Morse. A lower bound on convergence of a distributed network consensus algorithm. In *Proc. of IEEE Conf. on Decision & Control*, pages 2356–2361, Seville, Spain, 2005.

[14]M. Mesbahi and F. Hadaegh. Formation flying control of multiple spacecraft via graphs, matrix inequalities, and switching. *AIAA Journal of Guidance, Control, and Dynamics*, 24(2):369–377, 2001.

[15]Y. Song, Y. Li, and X. Liao. Orthogonal transformation based robust adaptive close formation control of multi-UAVs. In *Proc. of American Control Conf.*, pages 2983–2988, Portland, OR, 2005.

[16]D. Stipanovic, G. Inalhan, R. Teo, and C. Tomlin. Decentralized overlapping control of a formation of unmanned aerial vehicles. *Automatica*, 40(1):1285–1296, 2004.

[17]R. Ghabcheloo, P. Aguiar, A. Pascoal, C. Silvestre, I. Kaminer, and J. Hespanha. Coordinated path following control of autonomous underwater vehicles in presence of communication failures. In *Proc. of IEEE Conf. on Decision and Control*, San Diego, CA, 2006.

[18]F. Pereira and J. Sousa. Coordinated control of networked vehicles: An autonomous underwater system. *Automation and Remote Control*, 65(7):1037–1045, 2004.

[19]I. Kaminer, O. Yakimenko, V. Dobrokhodov, A. Pascoal, N. Hovakimyan, V. V. Patel, C. Cao, and A. Young. Coordinated path following for time-critical missions of multiple UAVs via $\mathcal{L}_1$ adaptive output feedback controllers. *AIAA Guidance, Navigation and Control Conference, AIAA 2007-6409, Hilton Head Island, SC*, August 2007.

[20]I. Kaminer, O. Yakimenko, A. Pascoal, and R. Ghabcheloo. Path generation, path following and coordinated control for timecritical missions of multiple UAVs. *American Control Conference*, pages 4906 – 4913, June 2006.

[21]V. Taranenko. *Experience of Ritz's, Puankare's and Ljapunov's Methods Utilization for Flight Dynamics Tasks Solution*. Air Force Engineering Academy Press, 1986.

[22]O. Yakimenko. Direct method for rapid prototyping of near-optimal aircraft trajectories. *AIAA Journal of Guidance, Control, & Dynamics*, 23(5):865–875, 2000.

[23]D. Soetanto, L. Lapierre, and A. Pascoal. Adaptive, non-singular path following, control of dynamic wheeled robots. In *Proc. ICAR*, Coimbra, Portugal, 2003.

[24]A. Micaelli and C. Samson. Trajectory-Tracking for Unicycle-Type and Two-Steering-Wheels Mobile Robot. Technical Report 2097, INRIA, Sophia-Antipolis, France, 1993.

[25]I. Kaminer, A. Pascoal, E. Xargay, C. Cao, N. Hovakimyan, and V. Dobrokhodov. 3D Path Following for Small UAVs using Commercial Autopilots augmented by $\mathcal{L}_1$ Adaptive Control. Submitted to *Journal of Guidance, Control and Dynamics*, 2008.

[26]N. Biggs. *Algebraic Graph Theory*. Cambridge University Press, 1993.

[27]H. K. Khalil. *Nonlinear Systems*. Third Edition, Prentice Hall, 2002.

[28]Z. Lin, B. Francis, and M. Maggiore. State agreement for continuous-time coupled nonlinear systems. *SIAM Journal of Control and Optimization*, 46(1):288–307, 2007.

[29]M. Arcak. Passivity as a desing tool for group coordination. *IEEE Trans. on Autom. Cont.*, 52(8):1380–1390, August 2007.

[30]C. Cao and N. Hovakimyan. Design and Analysis of a Novel $\mathcal{L}_1$ Adaptive Control Architecture with Guaranteed Transient Performance. *IEEE Transactions on Automatic Control*, 53(3):586–591, 2008.

[31]C. Cao and N. Hovakimyan. Guaranteed Transient Performance with $\mathcal{L}_1$ Adaptive Controller for Systems with Unknown Time-Varying Parameters and Bounded Disturbances: Part I. In *In Proc. of American Control Conference*, pages 3925–3930, New York, NY, July 2007.

[32]C. Cao and N. Hovakimyan. Stability Margins of $\mathcal{L}_1$ Adaptive Controller: Part II. In *In Proc. of American Control Conference*, pages 3931–3936, New York, NY, July 2007.

[33]J. B. Pomet and L. Praly. Adaptive Nonlinear Regulation: Estimation from the Lyapunov Equation. *IEEE Trans. Autom. Contr.*, 37(6):729–740, June 1992.

[34]C. Cao and N. Hovakimyan. $\mathcal{L}_1$ Adaptive Output Feedback Controller for Systems of Unknown Dimension. *IEEE Transactions on Automatic Control*, 53(3):815–821, April 2008.

[35]J. Burl. Piccolo/piccolo plus autopilots - a highly integrated autopilots for small UAVs. Cloud Cap Technology, Inc., `http://cloudcaptech.com/`.